important for integrin $\alpha_E\beta_7$ recognition, but not for homophilic adhesion, indicating that the E-cadherin residues critical for heterophilic adhesion to $\alpha_E\beta_7$ are distinct from those required for homophilic adhesion (32, 33). Higgins et al. (50) proposed a docking model involving the α_E A domain and EC1 in which the metal ion-dependent adhesion site cleft of α_E comes in contact with Glu^{31} of EC1 and the Phe^{298} projection of α_E coordinates with the hydrophobic pocket of EC1. Given a previous report showing that synthetic peptides encompassing Asn^{27}-Val^{34} in EC1 had very little inhibitory effect on the interaction with $\alpha_E\beta_7$ (32), however, full adhesive activity may require other binding sites or events, such as a conformational change in the cadherin or integrin molecules. Since domain 5 is located proximal to the membrane, it is less likely to serve as a direct binding site for the integrin, implying that the effect of the EC5 deletion on binding of the $\alpha_E\beta_7$ may be due to long-range effects that alter the conformation of more membrane distal domain of the molecules. However, the Δ5 mutants retained the ability to participate in homophilic adhesion and still bound the EC1-specific Ab SHE78-7 and the EC2-specific Ab HECD-1, indicating that a gross disruption of the conformation of the domain distal to EC5 is probably not occurring. The complexity of the EC5 conformational structure, containing asparagine residues of *N*-linked glycosylation and two intramolecular disulfide bonds, may favor the hypothesis that EC5 plays a role in the regulation of heterophilic adhesion via a change in conformation of the membrane proximal domain. Although the inside-out signaling mechanism that alters the conformational change in E-cadherin remains to be clarified, further functional and structural studies should provide an insight into our understanding of the role of EC5 in heterophilic adhesion. Identification of smaller deletions or point mutations in EC5 that also affected heterophilic adhesion by $\alpha_E\beta_7$ would be of considerable interest. The current data did not show that EC5-specific Ab G-10 block heterophilic adhesion of $\alpha_E\beta_7$ to E-cadherin. The adhesion was also not inhibited by the polyclonal Ab, which we newly generated in rabbits using a synthetic peptide corresponding to part of EC5 (our unpublished observations). If any anti-EC5 mAb blocks heterophilic adhesion to the same degree as anti-α_E, this would also be good supporting evidence for a role of EC5 in heterophilic adhesion.

Acknowledgments

We are grateful to Dr. D. Erle for providing K562-$\alpha_E\beta_7$ cells and Dr. Y. Shimoyama for providing the vector containing E-cadherin cDNA. We acknowledge the use of equipment belonging to the Saitama Medical School Research Center for Genomic Medicine

Disclosures

The authors have no financial conflict of interest.

References

1. Takeichi, M. 1991. Cadherin cell adhesion receptors as a morphogenetic regulator. *Science* 251: 1451–1455.
2. Takeichi, M. 1995. Morphogenetic roles of classical cadherins. *Curr. Opin. Cell Biol.* 7: 619–627.
3. Yap, A. S., W. M. Brieher, and B. M. Gumbiner. 1997. Molecular and functional analysis of cadherin-based adherens junctions. *Annu. Rev. Cell Dev. Biol.* 13: 119–146.
4. Nose, A., K. Tsuji, and M. Takeichi. 1990. Localization of specificity determining sites in cadherin cell adhesion molecules. *Cell* 61: 147–155.
5. Overduin, M., T. S. Harvey, S. Bagby, K. I. Tong, P. Yau, M. Takeichi, and M. Ikura. 1995. Solution structure of the epithelial cadherin domain responsible for selective cell adhesion. *Science* 267: 386–389.
6. Shapiro, L., A. M. Fannon, P. D. Kwong, A. Thompson, M. S. Lehmann, G. Grübel, J. F. Legrand, J. Als-Nielsen, D. R. Colman, and W. A. Hendrickson. 1995. Structural basis of cell-cell adhesion by cadherins. *Nature* 374: 327–337.
7. Makagiansar, I. T., P. D. Nguyen, A. Ikesue, K. Kuczera, W. Dentler, J. L. Urbauer, N. Galeva, M. Alterman, and T. J. Siahaan. 2002. Disulfide bond formation promotes the *cis*- and *trans*-dimerization of the E-cadherin-derived first repeat. *J. Biol. Chem.* 277: 16002–16010.
8. Blaschuk, O. W., R. Sullivan, S. David, and Y. Pouliot. 1990. Identification of a cadherin cell adhesion recognition sequence. *Dev. Biol.* 139: 227–229.
9. Noë, V., J. Willems, J. Vandekerckhove, F. van Roy, E. Bruyneel, and M. Mareel. 1999. Inhibition of adhesion and induction of epithelial cell invasion by HAV-containing E-cadherin-specific peptides. *J. Cell Sci.* 112: 127–135.
10. Boggon, T. J., J. Murray, S. Chappuis-Flament, E. Wong, B. M. Gumbiner, and L. Shapiro. 2002. C-cadherin ectodomain structure and implications for cell adhesion mechanisms. *Science* 296: 1308–1313.
11. Berx, G., K. F. Becker, H. Hofler, and F. van Roy. 1998. Mutations of the human E-cadherin (CDH1) gene. *Hum. Mutat.* 12: 226–237.
12. Mochado, J. C., P. Soares, F. Carneiro, A. Rocha, S. Beck, N. Blin, G. Berx, and M. Sobrinho-Simoes. 1999. E-cadherin gene mutations provide a genetic basis for the phenotypic divergence of mixed gastric carcinomas. *Lab. Invest.* 79: 459–465.
13. Endo, K., K. Ashida, N. Miyake, and T. Terada. 2001. E-cadherin gene mutations in human intrahepatic cholangiocarcinoma. *J. Pathol.* 193: 310–317.
14. Kremer, M., L. Quintanilla-Martinez, M. Fuchs, A. Gamboa-Dominguez, S. Haye, H. Kalthoff, E. Rosivatz, C. Hermannstadter, R. Busch, H. Hofler, and B. Luber. 2003. Influence of tumor-associated E-cadherin mutations on tumorigenicity and metastasis. *Carcinogenesis* 24: 1879–1886.
15. S. Chappuis-Flament, E. Wong, L. D. Hicks, C. M. Kay, and B. M. Gumbiner. 2001. Multiple cadherin extracellular repeats mediate homophilic binding and adhesion. *J. Cell Biol.* 154: 231–243.
16. Corada, M., F. Liao, M. Lindgren, M. G. Lampugnani, F. Breviario, R. Flank, W. A. Muller, D. J. Hicklin, P. Bohlen, and E. Dejana. 2001. Monoclonal antibodies directed to different regions of vascular endothelial cadherin extracellular domain affect adhesion and clustering of the protein and modulate endothelial permeability. *Blood* 97: 1679–1684.
17. Corada, M., L. Zanetta, F. Orsenigo, F. Breviario, M. G. Lampugnani, S. Bernasconi, F. Liao, D. J. Hicklin, P. Bohlen, and E. Dejana. 2002. A monoclonal antibody to vascular endothelial-cadherin inhibits tumor angiogenesis without side effects on endothelial permeability. *Blood* 100: 905–911.
18. Roberts, K., and P. J. Kilshaw. 1993. The mucosal T cell integrin $\alpha_{M290}\beta_7$ recognizes a ligand on mucosal epithelial cell lines. *Eur. J. Immunol.* 23: 1630–1635.
19. Cepek, K. L., C. M. Parker, J. L. Madara, and M. B. Brenner. 1993. Integrin $\alpha_E\beta_7$ mediates adhesion of T lymphocytes to epithelial cells. *J. Immunol.* 150: 3459–3470.
20. Cepek, K. L., S. K. Shaw, C. M. Parker, G. J. Russell, J. S. Morrow, D. L. Rimm, and M. B. Brenner. 1994. Adhesion between epithelial cells and T lymphocytes mediated by E-cadherin and the $\alpha_E\beta_7$ integrin. *Nature* 372: 190–193.
21. Karecla, P. I., S. J. Bowden, S. J. Green, and P. J. Kilshaw. 1995. Recognition of E-cadherin on epithelial cells by the mucosal T cell integrin $\alpha_{M290}\beta_7$ ($\alpha_E\beta_7$). *Eur. J. Immunol.* 25: 852–856.
22. Higgins, J. M. G., D. A. Mandlebrot, S. K. Shaw, G. J. Russel, E. A. Murphy,Y. T. Chen, W. J. Nelson, C. M. Parker, and M. B. Brenner. 1998. Direct and regulated interaction of integrin $\alpha_E\beta_7$ with E-cadherin. *J. Cell Biol.* 140: 197–210.
23. Kilshaw, P. J. 1999. $\alpha_E\beta_7$. *Mol. Pathol.* 52: 203–207.
24. Corps, E., C. Carter, P. Karecla, T. Ahrens, P. Evans, and P. Kilshaw. 2001. Recognition of E-cadherin by integrin $\alpha_E\beta_7$: requirement for cadherin dimerization and implications for cadherin and integrin function. *J. Biol. Chem.* 276: 30862–30870.
25. Cerf-Bensussan, N., A. Jarry, N. Brousse, B. Lisowska-Grospierre, D. Guy-Gland, and C. Griscelli. 1987. A monoclonal antibody (HML-1) defining a novel membrane molecule present on human intestinal lymphocytes. *Eur. J. Immunol.* 17: 1279–1285.
26. Rihs, S., C. Walker, J. C. Jr. Virchow, C. Boer, C. Kroegel, S. N. Giri, and R. K. Braun. 1996. Differential expression of $\alpha_E\beta_7$ integrins on bronchoalveolar lavage T lymphocyte subsets: regulation by $\alpha_4\beta_1$-integrin cross-linking and TGF-β. *Am. J. Respir. Cell Mol. Biol.* 15: 600–610.
27. Trollmo, C., I. M. Nilsson, C. Sollerman, and A. Tarkowski. 1996. Expression of the mucosal lymphocyte integrin $\alpha_E\beta_7$ and its ligand E-cadherin in the synovium of patients with rheumatoid arthritis. *Scand. J. Immunol.* 44: 293–298.
28. Kroneld, U., R. Jonsson, H. Carlsten, T. Bremell, A. C. Johannessen, and A. Tarkowski. 1998. Expression of the mucosal lymphocyte integrin $\alpha_E\beta_7$ and its ligand E-cadherin in salivary glands of patients with Sjögren's syndrome. *Scand. J. Rheumatol.* 27: 215–218.
29. Fujihara, T., H. Fujita, K. Tsubota, K. Saito, K. Tsuzaka, T. Abe, and T. Takeuchi. 1999. Preferential localization of $CD8^+$ $\alpha_E\beta_7{}^+$ T cells around acinar epithelial cells with apoptosis in patients with Sjögren's syndrome. *J. Immunol.* 163: 2226–2235.
30. Rottman, J. B., T. L. Smith, K. G. Ganley, T. Kikuchi, and J. G. Krueger. 2001. Potential role of the chemokine receptors CXCR3, CCR4, and the integrin $\alpha_E\beta_7$ in the pathogenesis of psoriasis vulgaris. *Lab. Invest.* 81: 335–347.
31. Teraki, Y., and T. Shiohara. 2002. Preferential expression of $\alpha_E\beta_7$ integrin (CD103) on $CD8^+$ T cells in the psoriatic epidermis: regulation by interleukins 4 and 12 and transforming growth factor-β. *Br. J. Dermatol.* 147: 1118–1126.
32. Karecla, P. I., S. J. Green, S. J. Bowden, J. Coadwell, and P. J. Kilshaw. 1996. Identification of a binding site for integrin $\alpha_E\beta_7$ in the N-terminal domain of E-cadherin. *J. Biol. Chem.* 271: 30909–30915.
33. Taraszka, K. S., J. M. G. Higgins, K. Tan, D. A. Mandelbrot, J. H. Wang, and M. B. Brenner. 2000. Molecular basis for leukocyte integrin $\alpha_E\beta_7$ adhesion to epithelial E-cadherin. *J. Exp. Med.* 191: 1555–1567.
34. Abitorabi, A. M., R. K. Pachynski, R. E. Ferrando, M. Tidswell, and D. J. Erle. 1997. Presentation of integrins on leukocyte microvilli: a role for the extracellular domain in determining membrane localization. *J. Cell Biol.* 139: 563–571.

35. Shimoyama, Y., H. Takeda, S. Yoshihara, M. Kitajima, and S. Hirohashi. 1999. Biochemical characterization and functional analysis of two type II classic cadherins, cadherin-6 and -14, and comparison with E-cadherin. *J. Biol. Chem.* 274: 11987–11994.
36. Pertz, O., D. Bozic, A. W. Koch, C. Fauser, A. Brancaccio, and J. Engel. 1999. A new crystal structure, Ca^{2+} dependence and mutational analysis reveal molecular details of E-cadherin homoassociation. *EMBO J.* 18: 1738–1747.
37. Renaud-Young, M., and W. J. Gallin. 2002. In the first extracellular domain of E-cadherin, heterophilic interactions, but not the conserved His-Ala-Val motif, are required for adhesion. *J. Biol. Chem.* 277: 39609–39616.
38. Ozawa, M., M. Ringwald, and R. Kemler. 1990. Uvomorulin-catenin complex formation is regulated by a specific domain in the cytoplasmic region of the cell adhesion molecule. *Proc. Natl. Acad. Sci. USA* 87: 4246–4250.
39. Brieher, W. M., A. S. Yap, and B. M. Gumbiner. 1996. Lateral dimerization is required for the homophilic binding activity of C-cadherin. *J. Cell Biol.* 135: 487–496.
40. Yap, A. S., C. M. Niessen, and B. M. Gumbiner. 1998. The juxtamembrane region of the cadherin cytoplasmic tail supports lateral clustering, adhesive strengthening, and interaction with $p120^{ctn}$. *J. Cell Biol.* 141: 779–789.
41. Huber, O., R. Kemler, and D. Langosch. 1999. Mutations affecting transmembrane segment interactions impair adhesiveness of E-cadherin. *J. Cell Sci.* 112: 4415–4423.
42. Ozawa, M. 2002. Lateral dimerization of the E-cadherin extracellular domain is necessary but not sufficient for adhesive activity. *J. Biol. Chem.* 277: 19600–19608.
43. Nelson, W. J., and R. Nesse. 2004. Convergence of Wnt, β-catenin, and cadherin pathways. *Science* 303: 1483–1487.
44. Williams, E. J., G. Williams, F. V. Howell, S. D. Skaper, F. S. Walsh, and P. Doherty. 2001. Identification of an N-cadherin motif that can interact with the fibroblast growth factor receptor and is required for axonal growth. *J. Biol. Chem.* 276: 43879–43886.
45. Corps, E. M., A. Robertson, M. J. Dauncey, and P. J. Kilshaw. 2003. Role of the αI domain in ligand binding by integrin $\alpha_E\beta_7$. *Eur. J. Immunol.* 33: 2599–2608.
46. Dransfield, I., C. Cabañas, A. Craig, and N. Hogg. 1992. Divalent cation regulation of the function of the leukocyte integrin LFA-1. *J. Cell Biol.* 116: 219–226.
47. Mould, A. P., J. A. Askari, S. Barton, A. D. Kline, P. A. McEwan, S. E. Craig, and M. J. Humphries. 2002. Integrin activation involves a conformational change in the α1 helix of the β subunit A-domain. *J. Biol. Chem.* 277: 19800–19805.
48. Takagi, J., B. M. Petre, T. Walz, and T. A. Springer. 2002. Global conformational rearrangements in integrin extracellular domains in outside-in and inside-out signaling. *Cell* 110: 599–511.
49. Pang, M., T. Abe, T. Fujihara, S. Mori, K. Tsuzaka, K. Amano, J. Koide, and T. Takeuchi. 1998. Up-regulation of $\alpha_E\beta_7$, a novel integrin adhesion molecule, on T cells from systemic lupus erythematosus patients with specific epithelial involvement. *Arthritis Rheum.* 41: 1456–1463.
50. Higgins, J. M. G., M. Cernadas, K. Tan, A. Irie, J. H. Wang, Y. Takada, and M. B. Brenner. 2000. The role of α and β chains in ligand recognition by β_7 integrins. *J. Biol. Chem.* 275: 25652–25664.

Serum-Free Spheroid Culture of Mouse Corneal Keratocytes

Satoru Yoshida,[1,2] *Shigeto Shimmura,*[1,3] *Jun Shimazaki,*[3] *Naoshi Shinozaki,*[1] *and Kazuo Tsubota*[1,3,4]

Purpose. To develop a serum-free mass culture system for mouse keratocytes.

Methods. Corneas of C57BL6/J mice were enzyme digested after the epithelium and endothelium were removed. Stromal cells were cultured in serum-free DMEM/F12 (1:1) containing epidermal growth factor (EGF), fibroblast growth factor 2 (FGF2), and B27 supplement. Primary spheres were dissociated by trypsin and subcultured as suspended secondary spheres. Cells from postnatal day (P)6 to P10 spheres were subcultured onto plastic dishes or type I collagen gels for phenotype analysis. The expression of the keratocyte markers keratocan, aldehyde dehydrogenase (Aldh), and CD34, were analyzed by RT-PCR, and vimentin and α-smooth muscle actin (α-SMA) were examined by immunocytochemistry.

Results. Primary keratocytes formed spheres, which were cultured for over 12 passages. Suspended sphere cells expressed vimentin, keratocan, CD34, and lumican, but were negative for cytokeratin K12 (K12) and Pax6. Sphere cells subcultured on plastic exhibited a dendritic morphology characteristic of keratocytes, and maintained keratocan, Aldh, and CD34 expression in serum-free medium. Sphere cells subcultured with 10% serum became fibroblastic, and expressed α-SMA when stimulated by transforming growth factor (TGF)-β. α-SMA-positive cells demonstrated contractile properties on collagen gels, compatible with the myofibroblast phenotype.

Conclusions. The phenotype of mouse keratocytes can be maintained in vitro for more than 12 passages by the serum-free sphere culturing technique. (*Invest Ophthalmol Vis Sci.* 2005;46:1653–1658) DOI:10.1167/iovs.04-1405

The corneal stroma is characterized by a well-organized extracellular matrix consisting of a dense network of collagen fibrils and proteoglycans that are produced by keratocytes, the principal stromal mesenchymal cell of cranial neural crest origin.[1,2] In adult tissue, keratocytes are mitotically quiescent cells with a flat, dendritic morphology. Keratocytes form a three-dimensional network of cells through their extensive dendritic processes, linked via gap junctions,[3–10] and secrete collagens and keratan sulfate proteoglycans such as lumican, mimecan, and keratocan.[11–15] The corneal stroma is rich in total keratan sulfate proteoglycan content,[16] but contain relatively small amounts of dermatan sulfate proteoglycans.[17]

During corneal wound healing, the quiescent keratocytes are activated and transform into fibroblasts and/or myofibroblasts, losing their characteristic dendritic morphology. Keratan sulfate proteoglycans are downregulated,[11,18] whereas keratocytes proliferate and migrate to the site of injury, causing scar formation.[19–22] The conversion to myofibroblasts, characterized by intense expression of the contractile protein α-smooth muscle actin (α-SMA),[21,23,24] is induced by endogenous and exogenous transforming growth factor (TGF)-β.[25–27]

Ex vivo expansion of keratocytes is often performed to investigate keratocytes in vitro, and various culture techniques have been reported involving the use of plastic substrates. However, when cultured in serum-containing medium, collagenase-isolated keratocytes from bovine[28] and rabbit[27,29] corneas readily lose their in vivo quiescent phenotype and acquire a fibroblastic phenotype with altered physiological properties.[28,30,31] In the presence of 2% to 10% serum, keratan sulfate proteoglycan production is greatly reduced or absent in keratocyte-derived fibroblasts,[28,32,33] whereas production of dermatan sulfate proteoglycans is upregulated. Furthermore, TGF-β stimulation or culture at low densities[30] causes corneal fibroblasts to differentiate further into myofibroblasts with a more spread-out morphology.[26,29,32,34] Serum-free cultures have been reported to be effective in the maintenance of the dendritic morphology of keratocytes and the production of keratan sulfate proteoglycans.[27,28,30–33,35,36] However, the cultivation of a large quantity of cells by subculturing has been difficult.

In this report, we introduce our method for subculturing mouse corneal keratocytes in large quantities, using a modified version of a suspension culture method originally described for neural stem cells.[37–39] In our study, the sphere culture of keratocytes did not require serum, and the dendritic keratocyte phenotype was restored when subcultured on plastic substrate in serum-free medium.

Materials and Methods

Cell Culture

All animals were handled in full accordance with the ARVO Statement for the Use of Animals in Ophthalmic and Vision Research. Stromal cells were dissociated from adult C57BL6/J mice (7–8 weeks old) and then cultured as described previously[40] with modifications. In brief, cornea tissue was excised in Hanks' balanced salt solution (HBSS) supplemented with 10% fetal bovine serum (FBS) by circular incision outside the limbus. The iris, ciliary body, and Descemet's membrane including the endothelium were bluntly dissected from the cornea. The remaining stroma with epithelium was incubated in 5 mg/mL of Dispase II (Roche Diagnostics, Indianapolis, IN) at 4°C overnight. Loose epithelial sheets were then removed, and corneal stromal discs were cut into small segments and digested in 0.05% trypsin (Sigma-Aldrich, St. Louis, MO) for 30 minutes at 37°C, followed by 78 U/mL

From the [1]Cornea Center and the [3]Department of Ophthalmology, Tokyo Dental College, Chiba, Japan; [2]SEED Co., Ltd, Tokyo, Japan; and the [4]Department of Ophthalmology, Keio University School of Medicine, Tokyo, Japan.

Supported in part by a grant for Advanced and Innovational Research Program in Life Sciences from the Ministry of Education, Culture, Sports, Science, and Technology of Japan.

Submitted for publication December 2, 2004; revised January 25, 2005; accepted January 26, 2005.

Disclosure: **S. Yoshida**, Seed Co., Ltd. (E); **S. Shimmura**, None; **J. Shimazaki**, None; **N. Shinozaki**, None; **K. Tsubota**, None

The publication costs of this article were defrayed in part by page charge payment. This article must therefore be marked "*advertisement*" in accordance with 18 U.S.C. §1734 solely to indicate this fact.

Corresponding author: Shigeto Shimmura, Department of Ophthalmology, Tokyo Dental College, 5-11-13 Sugano, Ichikawa 272-8513, Japan; shimmura@tdc.ac.jp.

TABLE 1. PCR Primers

Gene	Primer Sequence (5′–3′)	Product Size (bp)	GenBank Accession ID
Cytokeratin K12	Forward: TCCTCCTGCAGATTGACAACG Reverse: TTCCAGGGACGACTTCATGG	511	NM_010661
Pax6	Forward: AGTTCTTCGCAACCTGGCTA Reverse: TGAAGCTGCTGCTGATAGGA	500	NM_013627
Keratocan	Forward: AGGATGCCTTCATTCACGGAC Reverse: GCTCATTGTGGTGCTTATGGGG	491	NM_008438
Lumican	Forward: TGCTGTCTCGGCTTCTCTGAAAG Reverse: AACATCCCCCACATTCCCAACC	567	NM_008524
CD34	Forward: CCTTATTACACGGAGAATGGTGGAG Reverse: AAGAGGCGAGAGAGGAGAAATGGG	477	NM_133654
Vimentin	Forward: GAACGGAAAGTGGAATCCTTGC Reverse: GGTTGGCAGAGGCAGAGAAATC	591	NM_011701
Aldh	Forward: CTTCCAGCGGGTCATAAATCTG Reverse: AGCCAGCAAAACAAGTGTCAGG	528	NM_007436
Gapd	Forward: GACCACAGTCCATGCCATCAC Reverse: TCCACCACCCTGTTGCTGTAG	453	NM_008084

collagenase (Sigma-Aldrich) and 38 U/mL hyaluronidase (Sigma-Aldrich) for 30 minutes at 37°C.

Stromal cells were mechanically dissociated into single cells, and cultured in DMEM/F12 (1:1) supplemented with 20 ng/mL epidermal growth factor (EGF; Sigma-Aldrich), 10 ng/mL of fibroblast growth factor 2 (FGF2, Sigma-Aldrich), B27 supplement (Invitrogen, Carlsbad, CA), and 10^3 U/mL leukemia inhibitory factor (LIF; Chemicon International Inc., Temecula, CA) at a density of 5×10^5 cells/mL in a 37°C 5% CO_2 incubator. Initial culture was performed in 24-well plates or 35-mm dishes and then subcultured to 25-cm^2 culture flasks. The spheres were then further subcultured in 75 cm^2 culture flasks after 7 to 14 days, which was repeated every 7 to 14 days. Medium was changed every 5 to 7 days. All dishes and flasks used for sphere culture were polystyrene, noncoated vessels obtained from Asahi Techno Glass (Tokyo, Japan). Stromal sphere cells were examined by immunocytochemistry and RT-PCR. To allow cells to differentiate, cells dissociated from corneal spheres were cultured in serum-free or DMEM/F12 medium (10% FBS) supplemented with or without 2 ng/mL TGF-β (Sigma-Aldrich) for 4 days. Subcultured cells were stained by calcein-AM (Dojindo Laboratories, Tokyo, Japan), as described,[41] to visualize cell morphology. Primary stromal discs of mouse cornea were cultured in keratinocyte-serum free medium (K-SFM; Invitrogen) or DMEM/F12 with 10% FBS for 10 days (37°C, 5% CO_2), to identify any contamination by epithelial cells.

Immunocytochemistry

Immunocytochemistry was performed as described previously.[42] In brief, mouse corneal sphere cells and cells freshly isolated from mouse cornea were attached to glass slides by cytospin preparation (Auto Smear CF-120; Sakura, Tokyo, Japan) and then fixed in 4% paraformaldehyde for 15 minutes at 4°C. Cells were incubated in blocking serum for 30 minutes and then incubated with primary antibodies for 60 minutes. Primary antibodies used were anti-cytokeratin K12 (1:100, Santa Cruz Biotechnology, Santa Cruz, CA), anti-Pax6 (1:500, Chemicon International, Inc.), anti-vimentin (1:100, Santa Cruz Biotechnology), and anti-αSMA (1:200, Laboratory Vision, Fremont, CA). Immunoreactivity of primary antibodies was visualized with secondary antibodies conjugated with Cy3 or FITC (Jackson ImmunoResearch Laboratories, West Grove, PA).

Reverse Transcription–Polymerase Chain Reaction

Sphere cells and freshly dissociated corneal cells were collected and immediately frozen in liquid N_2. cDNAs were synthesized with a cDNA synthesis kit (Life Sciences, Inc., St. Petersburg, FL) from total RNA also prepared with a kit (RNeasy; Qiagen, Hilden, Germany). Gene-specific primers used for cytokeratin K12 (K12), Pax6, vimentin, keratocan, lumican, CD34, aldehyde dehydrogenase (Aldh), and Gapd are shown in Table 1. PCR was then performed (GeneAmp 9700; Applied Biosystems, Foster City, CA). The PCR products were analyzed by agarose gel electrophoresis.

Collagen Gel Contraction Assay

Collagen gel contraction assay was performed as described previously,[43–47] with some modifications. Collagen gels were prepared according to instructions provided by the manufacturer (Cellmaterix Type I-A; Nitta Gelatin, Osaka, Japan). In brief, collagen was mixed with 10-fold concentrated DMEM/F12 medium and 50 mM NaOH containing 260 mM $NaHCO_3$ and 200 mM HEPES at a proportion of 8:1:1 (vol/vol/vol) at 4°C. Then a 0.2-mL aliquot of the solution was placed in the center of each well of a six-well cell culture cluster (Corning Inc., Corning, NY) and allowed to polymerize at 37°C for 30 minutes in a cloning ring 10 mm in diameter (Asahi Techno Glass). Cells cultured in medium containing 10% FBS were harvested and suspended at 2×10^5 cells /mL. Eighty-five micrometers of the cell suspension was applied to a polymerized collagen gel and incubated overnight in a 37°C 5% CO_2 incubator. On day 1, the cloning ring was removed, and 2.5 mL of 10% FBS-containing medium was added to each well to submerge the cells. To examine TGF-β-dependent collagen gel contraction, TGF-β was added at a 0.1- or 1-ng/mL final concentration. As an inhibitor, an anti-TGF-β antibody (0.1 ng/mL) was also added in the medium for selected dishes. FBS-containing media with or without TGF-β and/or TGF-β antibody were changed on day 3. Gel thickness was measured on day 5 with an inverted phase-contrast microscope, by adjusting the plane of focus from the bottom to the top of the gel and recording the distance that the stage had been moved.

Data are expressed as the mean ± SD. Post hoc comparisons between groups was performed with the Tukey procedure. Differences were considered significant at $P < 0.01$.

RESULTS

Sphere Formation from Stromal Cells

More than five mice were used to prepare corneal stromal cells in each experiment. From 10 corneas, $1.32 \pm 0.16 \times 10^4$ cells ($n = 3$) were isolated, and subcultured cells proliferated into spheres, to yield an average of $7.97 \pm 0.35 \times 10^7$ cells per 75 cm^2 flask ($n = 6$) after four passages (P4). Sphere cells were propagated for >12 passages through 5 months without loss of viability. To avoid contamination of epithelial and endothelial cells, stromal discs were carefully prepared as described in the Materials and Methods sections. Dissociated cells from mouse stromal discs formed spheres when cultured in serum-free

medium containing EGF and FGF2 (Fig. 1A, left). To exclude the possibility that spheres may have originated from contaminating epithelial cells, we first performed primary cultures of mouse corneal discs, with or without dispase treatment, followed by epithelium separation. K-SFM with low Ca^{2+} was used to examine epithelial expansion.[48,49] When untreated discs were cultured, migration of epithelial and stromal cells was observed in K-SFM and in DMEM/F12 containing 10% FBS, respectively (Fig. 1B, left). There were no epithelial cells migrating from dispase-treated discs in both media, whereas fibroblasts migrated from the discs in DMEM/F12 with serum (Fig. 1B, right). We further cultured dissociated epithelial cells under conditions that allowed stromal spheres to form by 14 days. As a result, no spheres were observed in the epithelial cell culture (Fig. 1A, right). To demonstrate whether the spheres were hollow or solid, confocal microscopy of 4′,6′-diamino-2-phenylindole (DAPI)-stained spheres was performed. Imaging in different focal planes showed that the inside of spheres was filled with cells, not hollow (Fig. 1C).

We then examined the expression of epithelial and stromal markers in primary and subcultured spheres (P10) by RT-PCR. Stromal markers examined were the proteoglycans, keratocan, and lumican,[13,14,50,51] as well as CD34, which was recently reported to be expressed in keratocytes.[52–54] As shown in

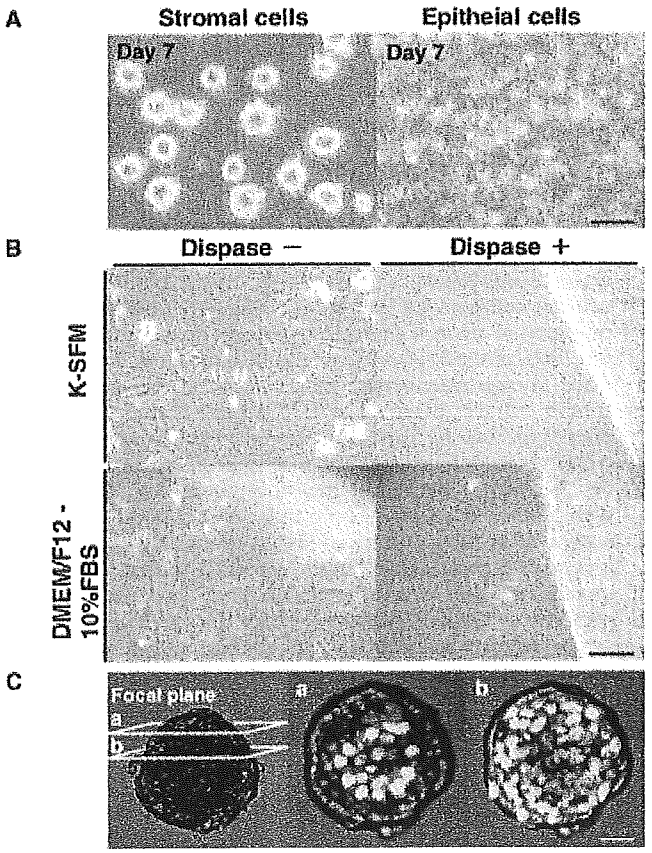

FIGURE 1. Sphere cells derived from the mouse corneal stroma. (A) Mouse corneal stroma and epithelium were separated by dispase treatment. Cells were cultured in DMEM/F12 supplemented with EGF and FGF2. After 7days' culture, spheres formed from stromal cells, but not from epithelial cells. (B) Mouse corneal discs were cultured in K-SFM or DMEM/F12 with 10% FBS. Epithelial cells migrated from intact corneal discs in K-SFM (*top left*) but not from dispase-treated (denuded) discs (*top right*). Expanding fibroblastic cells were still observed after dispase treatment. (C) Confocal images of the sphere in two different focal planes, a and b, as shown schematically (*left*). *Blue*: DAPI-stained nuclei. Scale bar: (A) 50 μm; (B) 100 μm; (C) 10 μm.

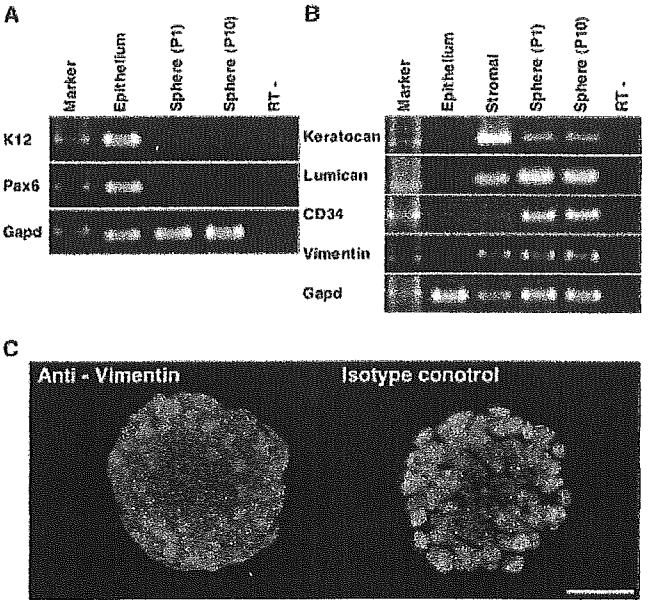

FIGURE 2. Sphere cells express keratocyte markers. (A, B) Total RNA was prepared from epithelial, stromal, and sphere cells. RT-PCR was performed with gene-specific primers. The epithelial markers K12 and Pax6 were not detected in the spheres (A). In contrast, the keratocyte markers keratocan, lumican, and CD34 were detected (B). Immunocytochemical analysis showed expression of the mesenchymal marker, vimentin, in spheres (C). *Blue*: nuclei of cells counterstained with DAPI. Scale bar, 50 μm.

Figures 2A and 2B, in addition to the mesenchymal intermediate filament vimentin, the expression of the genes described earlier were detected in the stromal spheres. On the contrary, K12 and Pax6, both of which are expressed in corneal epithelium,[40,42,55–58] were not detected in sphere cells (Fig. 2A).

Immunocytochemical analysis of spheres did not detect K12 and Pax6 expression (not shown), whereas vimentin staining was positive (Fig. 2C). These results show that sphere cells were of stromal, not epithelial, origin.

Characteristics of Sphere Cells

Sphere cells plated on collagen I-coated dishes in serum-free medium exhibited a dendritic morphology consistent with keratocytes (Fig. 3A).[3–10] RT-PCR showed that expression of keratocan and Aldh were retained under these conditions (Fig. 4). In contrast, the morphology of sphere cells subcultured in 10% serum were fibroblastic, and the expression of these genes was not detected (Fig. 4). Corneal sphere cells further differentiated to express α-SMA after exposure to TGF-β, which is consistent with the myofibroblast phenotype (Figs. 3C, 3D). Furthermore, when cells were subcultured on collagen gels in the presence of TGF-β, fibroblast-mediated gel contraction was observed (Fig. 5). Without TGF-β, contraction to 68.5% ± 1.75% of the original gel thickness was observed, whereas contraction was enhanced to 50.2% ± 3.96% or 29.4% ± 1.96% of the original thickness in the presence of 0.1 ng/mL or 1 ng of TGF-β, respectively ($P < 0.01$). TGF-β-dependent contraction was reduced to control levels when anti-TGF-β antibody was added to the medium.

Discussion

We successfully isolated and subcultured sphere-forming cells from the mouse corneal stroma, yielding a multifold increase in available cells for further experiments. Zhao et al.[40] have re-

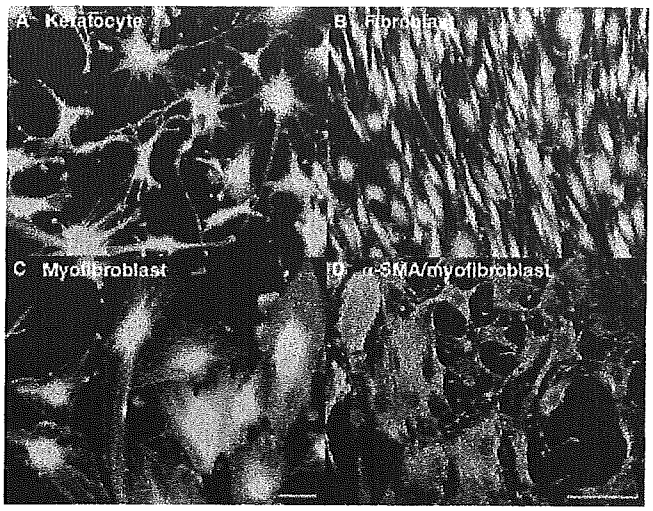

FIGURE 3. Phenotype of corneal stromal sphere cells stained by calcein-AM. Dissociated sphere cells were dendritic in SFM (**A**) and fibroblastic in adherent culture with medium containing 10% FBS (**B**). In the presence of TGF-β, morphology of adherent cells became myofibroblastic (**C**), and the cells expressed α-SMA, detected by immunocytochemistry (**D**, *green*). *Blue*: nuclei of cells counterstained with DAPI. Scale bar, 50 μm.

ported that cells present in limbus-derived spheres are derived from the limbal epithelium but not the stroma. However, the corneal sphere cells that we isolated did not express the epithelial markers K12 or Pax6 throughout the study, and furthermore, exhibited properties of corneal keratocytes when subcultured in serum-free medium. The morphology of the subcultured cells as shown in Figure 3 was similar to that of keratocytes in situ, and together with the expression of keratocan, lumican, Aldh, and CD34 in the subcultured cells, the

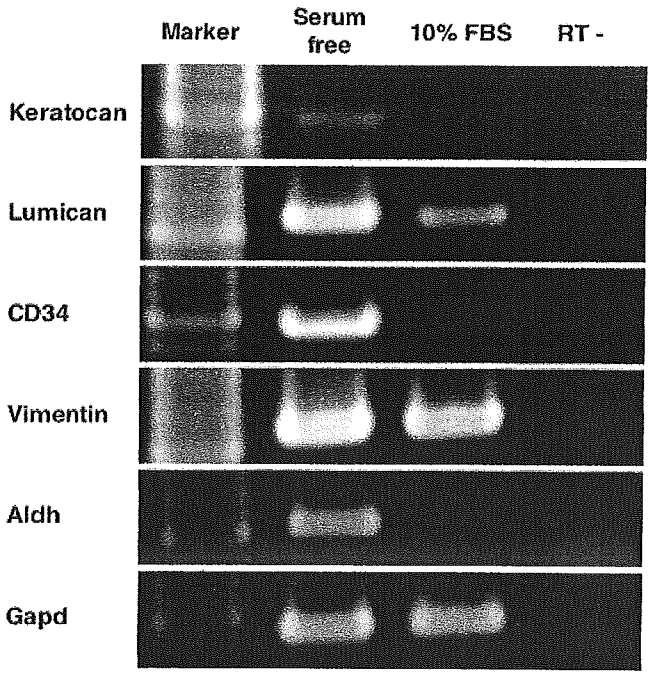

FIGURE 4. RT-PCR analysis of keratocyte markers expressed in sphere cells subcultured on plastic. Keratocan and Aldh were expressed only in cells in SFM, whereas lumican, CD34, and vimentin were also detected in cells cultured in the presence of 10% FBS.

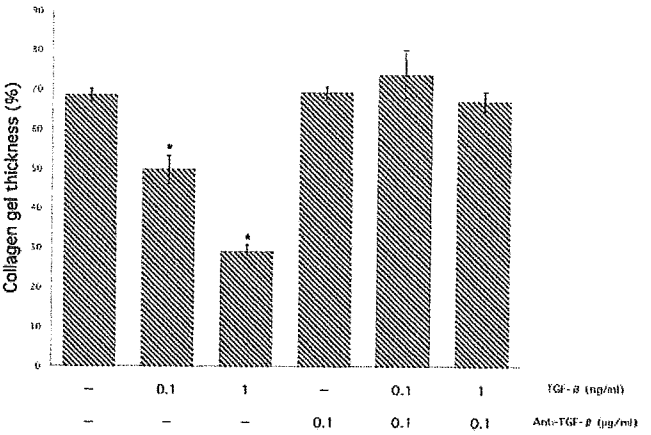

FIGURE 5. Collagen gel contraction assay of fibroblasts. Mouse corneal spheres were allowed to differentiate in 10% serum-containing medium. Dose-dependent TGF-β-induced collagen gel contraction was observed, which was inhibited by an anti-TGF-β antibody ($^*P < 0.01$).

collective evidence shows that these cells were of keratocyte origin. Although most genes were expressed during sphere cultures and maintained after adhesion to plastic dishes, keratocan, and Aldh were exclusively expressed in the keratocyte phenotype in serum-free medium (Fig. 4). Although the biological role of Aldh is not known, abundant expression of the water-soluble enzyme was shown to be expressed in the keratocyte phenotype, but not by the fibroblasts or myofibroblasts.[32,59]

Plated sphere cells can further be induced to differentiate into the fibroblast and myofibroblast phenotypes. Sphere cells seeded onto plastic in the presence of 10% serum exhibited the morphology and properties of stromal fibroblasts.[28] The transition to α-SMA-positive myofibroblasts by exposure to TGF-β, causing collagen gel contraction (Fig. 5), is also a functional property of stromal fibroblast primary cultures.[29,43,60] Therefore, subcultured sphere cells can be conditioned to express all three known phenotypes of keratocytes after expansion by sphere culture. Berryhill et al.[36] reported that the fibroblast phenotype can be partially restored to the keratocyte phenotype in terms of extracellular matrix production and morphology. However, biological functions, including Aldh activity, were not restored, suggesting that reversal to keratocyte phenotype after mass culture in serum-containing medium is not practical. Espana et al.[41] have reported the use of amniotic membrane (AM) as a substrate for keratocyte cultures in the presence of serum. They have shown that even with the use of serum, primary keratocytes maintained dendritic morphology on AM. The expression of keratocan and lumican was also present for up to five passages, which is a significant improvement over previous reports using artificial substrates. Still, the scarcity of keratocytes in tissue usually necessitates the use of human tissue or cells from larger animals, such as cows,[28,36] rabbits,[30] and rhesus monkeys.[61] Biochemical and molecular analysis of such cells are difficult due to the lack of available antibodies and genomic information.

During subcultures of spheres, cells that failed to form spheres were found attached to the dish as nondividing, fibroblast-like cells (data not shown). Although these cells may have had low viability, there may be a selection process that allows only cells with high growth potential to propagate as spheres. Once secondary spheres are successfully initiated, subsequent passages continue to produce spheres for at least 12 passages, the longest that we observed. To our surprise, cells from later passages continued to show the keratocyte phenotype when subcultured on plastic, suggesting the possible presence of

committed progenitor cells during the sphere culture stage. Many aspects of the keratocyte are still not understood, and the availability of cells from the mouse cornea should be a powerful tool in studying the biology of these cells.

Acknowledgments

The authors thank Kimie Katoh for technical assistance and all members of the Cornea Center Laboratory for helpful suggestions.

References

1. Bard JB, Hay ED. The behavior of fibroblasts from the developing avian cornea: morphology and movement in situ and in vitro. *J Cell Biol.* 1975;67:400–418.
2. Lwigale PY, Conrad GW, Bronner-Fraser M. Graded potential of neural crest to form cornea, sensory neurons and cartilage along the rostrocaudal axis. *Development.* 2004;131:1979–1991.
3. Poole CA, Brookes NH, Clover GM. Confocal imaging of the human keratocyte network using the vital dye 5-chloromethylfluorescein diacetate. *Clin Exp Ophthalmol.* 2003;31:147–154.
4. Poole CA, Brookes NH, Clover GM. Keratocyte networks visualised in the living cornea using vital dyes. *J Cell Sci.* 1993;106:685–691.
5. Poole CA, Brookes NH, Clover GM. Confocal imaging of the keratocyte network in porcine cornea using the fixable vital dye 5-chloromethylfluorescein diacetate. *Curr Eye Res.* 1996;15:165–174.
6. Jester JV, Barry PA, Lind GJ, Petroll WM, Garana R, Cavanagh HD. Corneal keratocytes: in situ and in vitro organization of cytoskeletal contractile proteins. *Invest Ophthalmol Vis Sci.* 1994;35:730–743.
7. Zieske JD, Guimaraes SR, Hutcheon AE. Kinetics of keratocyte proliferation in response to epithelial debridement. *Exp Eye Res.* 2001;72:33–39.
8. Hahnel C, Somodi S, Slowik C, Weiss DG, Guthoff RF. Fluorescence microscopy and three-dimensional imaging of the porcine corneal keratocyte network. *Graefes Arch Clin Exp Ophthalmol.* 1997;235:773–779.
9. Watsky MA. Keratocyte gap junctional communication in normal and wounded rabbit corneas and human corneas. *Invest Ophthalmol Vis Sci.* 1995;36:2568–2576.
10. Ueda A, Nishida T, Otori T, Fujita H. Electron-microscopic studies on the presence of gap junctions between corneal fibroblasts in rabbits. *Cell Tissue Res.* 1987;249:473–475.
11. Carlson EC, Wang IJ, Liu CY, Brannan P, Kao CW, Kao WW. Altered KSPG expression by keratocytes following corneal injury. *Mol Vis.* 2003;9:615–623.
12. Michelacci YM. Collagens and proteoglycans of the corneal extracellular matrix. *Braz J Med Biol Res.* 2003;36:1037–1046.
13. Kao WW, Liu CY. Roles of lumican and keratocan on corneal transparency. *Glycoconj J.* 2002;19:275–285.
14. Liu CY, Birk DE, Hassell JR, Kane B, Kao WW. Keratocan-deficient mice display alterations in corneal structure. *J Biol Chem.* 2003; 278:21672–21677.
15. Dunlevy JR, Beales MP, Berryhill BL, Cornuet PK, Hassell JR. Expression of the keratan sulfate proteoglycans lumican, keratocan and osteoglycin/mimecan during chick corneal development. *Exp Eye Res.* 2000;70:349–362.
16. Funderburgh JL, Caterson B, Conrad GW. Distribution of proteoglycans antigenically related to corneal keratan sulfate proteoglycan. *J Biol Chem.* 1987;262:11634–11640.
17. Hassell JR, Cintron C, Kublin C, Newsome DA. Proteoglycan changes during restoration of transparency in corneal scars. *Arch Biochem Biophys.* 1983;222:362–369.
18. Sundarraj N, Fite D, Belak R, et al. Proteoglycan distribution during healing of corneal stromal wounds in chick. *Exp Eye Res.* 1998; 67:433–442.
19. Matsuda H, Smelser GK. Electron microscopy of corneal wound healing. *Exp Eye Res.* 1973;16:427–442.
20. Cintron C, Hassinger LC, Kublin CL, Cannon DJ. Biochemical and ultrastructural changes in collagen during corneal wound healing. *J Ultrastruct Res.* 1978;65:13–22.
21. Garana RM, Petroll WM, Chen WT, et al. Radial keratotomy. II. Role of the myofibroblast in corneal wound contraction. *Invest Ophthalmol Vis Sci.* 1992;33:3271–3282.
22. Fini ME. Keratocyte and fibroblast phenotypes in the repairing cornea. *Prog Retin Eye Res.* 1999;18:529–551.
23. Jester JV, Petroll WM, Barry PA, Cavanagh HD. Expression of alpha-smooth muscle (alpha-SM) actin during corneal stromal wound healing. *Invest Ophthalmol Vis Sci.* 1995;36:809–819.
24. Jester JV, Huang J, Barry-Lane PA, Kao WW, Petroll WM, Cavanagh HD. Transforming growth factor(beta)-mediated corneal myofibroblast differentiation requires actin and fibronectin assembly. *Invest Ophthalmol Vis Sci.* 1999;40:1959–1967.
25. Petroll WM, Jester JV, Barry-Lane PA, Cavanagh HD. Effects of basic FGF and TGF beta 1 on F-actin and ZO-1 organization during cat endothelial wound healing. *Cornea.* 1996;15:525–532.
26. Petridou S, Masur SK. Immunodetection of connexins and cadherins in corneal fibroblasts and myofibroblasts. *Invest Ophthalmol Vis Sci.* 1996;37:1740–1748.
27. Jester JV, Barry-Lane PA, Cavanagh HD, Petroll WM. Induction of alpha-smooth muscle actin expression and myofibroblast transformation in cultured corneal keratocytes. *Cornea.* 1996;15:505–516.
28. Beales MP, Funderburgh JL, Jester JV, Hassell JR. Proteoglycan synthesis by bovine keratocytes and corneal fibroblasts: maintenance of the keratocyte phenotype in culture. *Invest Ophthalmol Vis Sci.* 1999;40:1658–1663.
29. Jester JV, Ho-Chang J. Modulation of cultured corneal keratocyte phenotype by growth factors/cytokines control in vitro contractility and extracellular matrix contraction. *Exp Eye Res.* 2003;77: 581–592.
30. Masur SK, Dewal HS, Dinh TT, Erenburg I, Petridou S. Myofibroblasts differentiate from fibroblasts when plated at low density. *Proc Natl Acad Sci USA.* 1996;93:4219–4223.
31. Long CJ, Roth MR, Tasheva ES, et al. Fibroblast growth factor-2 promotes keratan sulfate proteoglycan expression by keratocytes in vitro. *J Biol Chem.* 2000;275:13918–13923.
32. Funderburgh JL, Mann MM, Funderburgh ML. Keratocyte phenotype mediates proteoglycan structure: a role for fibroblasts in corneal fibrosis. *J Biol Chem.* 2003;278:45629–45637.
33. Funderburgh JL, Funderburgh ML, Mann MM, Prakash S, Conrad GW. Synthesis of corneal keratan sulfate proteoglycans by bovine keratocytes in vitro. *J Biol Chem.* 1996;271:31431–31436.
34. Funderburgh JL, Funderburgh ML, Mann MM, Corpuz L, Roth MR. Proteoglycan expression during transforming growth factor beta-induced keratocyte-myofibroblast transdifferentiation. *J Biol Chem.* 2001;276:44173–44178.
35. Berryhill BL, Beales MP, Hassell JR. Production of prostaglandin D synthase as a keratan sulfate proteoglycan by cultured bovine keratocytes. *Invest Ophthalmol Vis Sci.* 2001;42:1201–1207.
36. Berryhill BL, Kader R, Kane B, Birk DE, Feng J, Hassell JR. Partial restoration of the keratocyte phenotype to bovine keratocytes made fibroblastic by serum. *Invest Ophthalmol Vis Sci.* 2002;43: 3416–3421.
37. Reynolds BA, Weiss S. Generation of neurons and astrocytes from isolated cells of the adult mammalian central nervous system. *Science.* 1992;255:1707–1710.
38. Reynolds BA, Tetzlaff W, Weiss S. A multipotent EGF-responsive striatal embryonic progenitor cell produces neurons and astrocytes. *J Neurosci.* 1992;12:4565–4574.
39. Milward EA, Lundberg CG, Ge B, Lipsitz D, Zhao M, Duncan ID. Isolation and transplantation of multipotential populations of epidermal growth factor-responsive, neural progenitor cells from the canine brain. *J Neurosci Res.* 1997;50:862–871.
40. Zhao X, Das AV, Thoreson WB, et al. Adult corneal limbal epithelium: a model for studying neural potential of non-neural stem cells/progenitors. *Dev Biol.* 2002;250:317–331.
41. Espana EM, He H, Kawakita T, et al. Human keratocytes cultured on amniotic membrane stroma preserve morphology and express keratocan. *Invest Ophthalmol Vis Sci.* 2003;44:5136–5141.
42. Davis J, Duncan MK, Robison WG Jr, Piatigorsky J. Requirement for Pax6 in corneal morphogenesis: a role in adhesion. *J Cell Sci.* 2003;116:2157–2167.
43. Nakamura K. Interaction between injured corneal epithelial cells and stromal cells. *Cornea.* 2003;22:S35–S47.

44. Kurosaka H, Kurosaka D, Kato K, Mashima Y, Tanaka Y. Transforming growth factor-beta 1 promotes contraction of collagen gel by bovine corneal fibroblasts through differentiation of myofibroblasts. *Invest Ophthalmol Vis Sci.* 1998;39:699–704.
45. Guidry C, McFarland RJ, Morris R, Witherspoon CD, Hook M. Collagen gel contraction by cells associated with proliferative vitreoretinopathy. *Invest Ophthalmol Vis Sci.* 1992;33:2429–2435.
46. Asaga H, Kikuchi S, Yoshizato K. Collagen gel contraction by fibroblasts requires cellular fibronectin but not plasma fibronectin. *Exp Cell Res.* 1991;193:167–174.
47. Guidry C, Grinnell F. Contraction of hydrated collagen gels by fibroblasts: evidence for two mechanisms by which collagen fibrils are stabilized. *Coll Relat Res.* 1987;6:515–529.
48. Bertolero F, Kaighn ME, Gonda MA, Saffiotti U. Mouse epidermal keratinocytes: clonal proliferation and response to hormones and growth factors in serum-free medium. *Exp Cell Res.* 1984;155:64–80.
49. Kawakita T, Espana EM, He H, Yeh LK, Liu CY, Tseng SC. Calcium-induced abnormal epidermal-like differentiation in cultures of mouse corneal-limbal epithelial cells. *Invest Ophthalmol Vis Sci.* 2004;45:3507–3512.
50. Liu CY, Shiraishi A, Kao CW, et al. The cloning of mouse keratocan cDNA and genomic DNA and the characterization of its expression during eye development. *J Biol Chem.* 1998;273:22584–22588.
51. Corpuz LM, Funderburgh JL, Funderburgh ML, Bottomley GS, Prakash S, Conrad GW. Molecular cloning and tissue distribution of keratocan: bovine corneal keratan sulfate proteoglycan 37A. *J Biol Chem.* 1996;271:9759–9763.
52. Espana EM, Kawakita T, Liu CY, Tseng SC. CD-34 expression by cultured human keratocytes is downregulated during myofibroblast differentiation induced by TGF-beta1. *Invest Ophthalmol Vis Sci.* 2004;45:2985–2991.
53. Joseph A, Hossain P, Jham S, et al. Expression of CD34 and L-selectin on human corneal keratocytes. *Invest Ophthalmol Vis Sci.* 2003;44:4689–4692.
54. Toti P, Tosi GM, Traversi C, Schurfeld K, Cardone C, Caporossi A. CD-34 stromal expression pattern in normal and altered human corneas. *Ophthalmology.* 2002;109:1167–1171.
55. Koroma BM, Yang JM, Sundin OH. The Pax-6 homeobox gene is expressed throughout the corneal and conjunctival epithelia. *Invest Ophthalmol Vis Sci.* 1997;38:108–120.
56. Liu CY, Zhu G, Westerhausen-Larson A, et al. Cornea-specific expression of K12 keratin during mouse development. *Curr Eye Res.* 1993;12:963–974.
57. Shiraishi A, Converse RL, Liu CY, Zhou F, Kao CW, Kao WW. Identification of the cornea-specific keratin 12 promoter by in vivo particle-mediated gene transfer. *Invest Ophthalmol Vis Sci.* 1998;39:2554–2561.
58. Liu JJ, Kao WW, Wilson SE. Corneal epithelium-specific mouse keratin K12 promoter. *Exp Eye Res.* 1999;68:295–301.
59. Jester JV, Møller-Pedersen T, Huang J, et al. The cellular basis of corneal transparency: evidence for 'corneal crystallins.' *J Cell Sci.* 1999;112:613–622.
60. Stramer BM, Zieske JD, Jung JC, Austin JS, Fini ME. Molecular mechanisms controlling the fibrotic repair phenotype in cornea: implications for surgical outcomes. *Invest Ophthalmol Vis Sci.* 2003;44:4237–4246.
61. Hassell JR, Newsome DA, Hascall VC. Characterization and biosynthesis of proteoglycans of corneal stroma from rhesus monkey. *J Biol Chem.* 1979;254:12346–12354.

Available online at www.sciencedirect.com
SCIENCE DIRECT®
Biochemical and Biophysical Research Communications 327 (2005) 100–105
BBRC
www.elsevier.com/locate/ybbrc

SOCS3/CIS3 negative regulation of STAT3 in HGF-induced keratinocyte migration

Sho Tokumaru[a], Koji Sayama[a,*], Kenshi Yamasaki[a], Yuji Shirakata[a], Yasushi Hanakawa[a], Yoko Yahata[a], Xiuju Dai[a], Mikiko Tohyama[a], Lujun Yang[a], Akihiko Yoshimura[b], Koji Hashimoto[a]

[a] *Department of Dermatology, Ehime University School of Medicine, Ehime, Japan*
[b] *Division of Molecular and Cellular Immunology, Medical Institute of Bioregulation, Kyusyu University, Fukuoka, Japan*

Received 20 November 2004
Available online 9 December 2004

Abstract

Hepatocyte growth factor (HGF) is a potent mitogen for mature hepatocytes. Because HGF has strong effects on the motility of keratinocytes and is produced by fibroblasts, HGF is thought to regulate keratinocyte migration during wound healing. However, the intracellular signaling mechanism of HGF-induced keratinocyte migration is poorly understood. In this report, we clarify the roles of STAT3 and SOCS/CIS family in HGF-induced keratinocyte migration. HGF activated STAT3 and strongly induced keratinocyte migration. Transfection with the dominant-negative mutant of STAT3 almost completely abolished HGF-induced keratinocyte migration and STAT3 phosphorylation. Next, we studied the mechanisms that regulate STAT3 phosphorylation. HGF enhanced the expression of SOCS3/CIS3 by sixfold within 1 h, but had minimum effect on SOCS1/JAB expression. Transfection with SOCS3/CIS3 almost completely abolished HGF-induced STAT3 phosphorylation and keratinocyte migration, indicating that SOCS3/CIS3 acts as a negative regulator of HGF-induced keratinocyte migration. In conclusion, SOCS3/CIS3 regulates HGF-induced keratinocyte migration by inhibiting STAT3 phosphorylation.

Keywords: Keratinocytes; HGF; Migration; STAT3; STAT1; SOCS3/CIS3; SOCS1/JAB; Wound healing; Adenovirus vector

The migration of epidermal keratinocytes is an important step in skin wound healing. Several growth factors regulate keratinocyte migration [1]. Hepatocyte growth factor (HGF) is a potent mitogen for mature hepatocytes [2,3]. HGF also has mitogenic, motogenic, morphogenic, and tumor-inhibitory activities for a variety of cells, including epithelial, endothelial, and some types of stromal cells [4–6]. Because HGF has potent effects on the motility of keratinocytes and because dermal fibroblasts produce HGF in the skin [7], HGF has been suggested to play a regulatory role in keratinocyte migration during wound healing [8,9]. Recently, an application of HGF has been demonstrated as a potential therapeutic approach for the treatment of cutaneous ulcer [10–13]. However, the intracellular signaling mechanism of HGF-induced migration is poorly understood.

c-Met is an HGF receptor that is autophosphorylated upon binding of HGF. Phosphorylated c-Met recruits a number of substrates with Src homology (SH)2 domains, such as phosphatidylinositol 3-kinase [14], Grb-2 (ASH)/Sos complex [15], Ras GTPase activating protein, $pp60^{src}$, and phospholipase C [15]. Grb-2 has also been implicated in the recruitment of the large adaptor protein Grb-2-associated binding protein-1 (Gab1) to the Met signaling complex [16–18]. These signaling molecules lead to mitogenic activity via the Ras–Raf1–MEK–MAPK pathway. In addition to these

* Corresponding author. Fax: +81 960 5352.
E-mail address: sayama@m.ehime-u.ac.jp (K. Sayama).

0006-291X/$ - see front matter © 2004 Elsevier Inc. All rights reserved.
doi:10.1016/j.bbrc.2004.11.145

pathways, two signal transducers and activators of transcription (STAT) proteins, STAT1 and STAT3, are signaling cascade proteins located downstream from c-Met [19].

The STAT signaling pathways are negatively regulated by proteins of the suppressor of cytokine signaling (SOCS)/cytokine-inducible SH2-containing protein (CIS) family to avoid oversignaling [20]. The SOCS/CIS family is induced by cytokine stimulation and binds to tyrosine-phosphorylated sites of the cytokine receptor or to Jak through an SH2 domain, resulting in the inhibition of tyrosine kinase phosphorylation. CIS was the first member of the SOCS/CIS family to be identified; it binds to the tyrosine-phosphorylated site of the erythropoietin receptor and inhibits the STAT5 signal downstream [21]. Additional members of the SOCS/CIS family have been identified independently [22,23]. SOCS1/JAB binds mainly to Jak2 [24] and regulates the IFN-γ/STAT1 [25] and IL-6/STAT3 signaling pathways [23]. SOCS2/CIS2 regulates insulin-like growth factor and the insulin-like growth factor receptor signaling pathways [26]. SOCS3/CIS3 regulates the IL-6/STAT3 and IFN-γ/STAT1 signaling pathways.

Because STATs are involved in the HGF-c-Met signaling pathway, we hypothesized that the SOCS/CIS family regulates HGF-induced keratinocyte migration by inhibiting STAT pathways. To prove this, we first studied whether STAT3 was involved in HGF-induced keratinocyte migration. Next, we tested whether the SOCS/CIS family affects HGF-induced keratinocyte migration through the inhibition of STAT3.

Materials and methods

Reagents and antibodies. Recombinant HGF was kindly provided by Dr. Kunio Matsumoto (Osaka University, Osaka, Japan). Antibodies were purchased as follows: mouse monoclonal STAT3 (Transduction Laboratories) and phospho-STAT3 (New England Biolabs).

Keratinocyte culture. Human skin samples were obtained after plastic surgery under a protocol approved by the Institutional Review Board of Ehime University School of Medicine. Primary normal human keratinocytes were isolated from the normal human skin. Normal human keratinocytes were cultured with MCDB153 medium supplemented with insulin (1 μg/ml), hydrocortisone (0.5 μM), ethanolamine (0.1 mM), phosphoethanolamine (0.1 mM), bovine hypothalamic extract (BHE; 50 μg/ml), and Ca^{2+}(0.1 mM). This supplement was as described elsewhere [27].

Migration assay. Keratinocytes were cultured at 1×10^5 cells per 35-mm type I-collagen-coated culture plate in culture medium without BHE for 12 h. After stimulation, keratinocyte migration was observed using time-lapse video microscopy (IX-IBC, CK30; Olympus, Tokyo, Japan) in a controlled chamber at 37 °C and 5% CO_2.

Keratinocyte migration was assayed quantitatively with a Boyden chamber, as previously described [28]. Designated amounts of HGF were added to the bottom wells of a 48-well Boyden chamber (Neuro Probe, Cabin John, MD), and an 8-μm pore-size polyvinylpyrrolidone-free polycarbonate membrane (Neuro Probe) was placed on the wells. The membrane was precoated with type I collagen (10 μg/ml in PBS, Nitta Gelatin, Osaka, Japan) at room temperature for 1 h and then extensively washed with PBS. Subconfluent keratinocytes were harvested with trypsin–EDTA (0.05% trypsin and 0.5 mM EDTA) and resuspended in the culture medium without BHE at 1×10^5 cells/ml. Fifty microliters of the keratinocyte suspension (5000 cells/well) was added to the upper wells, and the chamber was incubated overnight at 37 °C in a humidified atmosphere of air with 5% CO_2. Cells that adhered to the upper surface of the filter membrane were removed by scraping with a rubber blade. Cells that moved through the filter and stayed on the lower surface of the membrane were considered to be migrated cells. The membrane was fixed with 10% buffered formalin overnight and then stained with Gill's hematoxylin overnight. The membrane was then mounted between two glass slides with 90% glycerol and the number of migrated cells was determined by counting under a microscope.

Western blotting. Subconfluent keratinocytes were starved for 2 h in BHE-free medium and stimulated with HGF as indicated. Cells were harvested on ice in lysis buffer containing 5 mM EDTA, 100 μM sodium orthovanadate, 100 μM sodium pyrophosphate, 1 mM sodium fluoride, 5 μM 3,4-dichloroisocoumarin, 1 μg/ml aprotinin, and 1% Triton X-100 in PBS. Twenty micrograms of protein was separated on 10% SDS–PAGE and then transferred to a PVDF membrane. The membranes were blocked with 5% skimmed milk in PBS overnight at 4 °C. The blocked membranes were incubated for 6 h with the first antibody as indicated. After three washes with PBS containing 0.05% Tween 20, the membranes were treated with ABC reagents (VECTOR Laboratories, Burlingame, CA) for 20 min at room temperature, washed three times with PBS containing 0.05% Tween 20, treated with ECL detection reagents (Amersham–Pharmacia Biotech, Piscataway, NJ) for 1 min at room temperature, and then exposed to films (Kodak, Rochester, NY).

Quantitative PCR analysis. Total RNA from cultured human keratinocytes was prepared using Isogen (Nippon Gene, Toyama, Japan) and was treated with 50 U/ml DNase I (Clontech) at 37 °C for 30 min to remove any genomic DNA contamination.

To quantify the mRNA expression in vivo, we performed quantitative RT-PCR using the ABI Prism 7700 sequencer detection system (Perkin–Elmer Applied Biosystems, Foster City, CA). RT-PCR mixtures were prepared according to the manufacturer's instructions for the TaqMan One-Step RT-PCR Master Mix Reagent kit (Perkin–Elmer Applied Biosystems). Briefly, 50 ng of total RNA was added to each 50-μl reaction mixture containing 1 μl master mix, 1× multiScribe and RNase inhibitor mix, 200 nM of each primer, and 100 nM hybridization probe for specific detection of target cDNA. For SOCS1/JAB detection, the sense primer 5′-TTTTTCGCCCTTAGC GTGAA-3′, the antisense primer 5′-GCCATCCAGGTGAAAGCG-3′, and the probe 5′-CCTCGGGACCCACGAGCATCC-3′ were added. For SOCS3/CIS3 detection, the sense primer 5′-TTCAGCA TCTCTGTCGGAAGAC-3′, the antisense primer 5′-GCATCGTAC TGGTCCAGGAACT-3′, and the probe 5′-AACGGCCACCTGG ACTCCTATGAGAAA-3′ were added. The probe was labeled with a reporter fluorescent dye, FAM (6-carboxyfluorescein), at the 5′-end. For GAPDH detection, 1 μl of Pre-Developed TaqMan Assay Reagent (Perkin–Elmer Applied Biosystems) was added. The thermal conditions were 48 °C for 30 min for reverse transcription and 95 °C for 10 min, followed by 45 amplification cycles of 95 °C for 15 s for denaturing and 55 °C for 1.5 min for annealing and extension. The PCR products were sequenced to confirm the proper amplification. To compare mRNA expression, the results were estimated as relative values using GAPDH as an internal reference. The relative quantified expression was calculated using the following formula: relative expression $= 2[-(\sum CT_s/N_s - \sum CT_{GAPDH_s}/N_s) - (\sum CT_r/N_r - \sum CT_{GAPDH_r}/N_r)]$, where CT_s denotes the cycle threshold for the candidate gene in the sample, N_s is the number of samples, CT_{GAPDH_s} is the cycle threshold for GAPDH in the same sample, CT_r is the cycle threshold for the candidate gene in the overall reference sample, N_r is the number of reference samples, and CT_{GAPDH_r} is the cycle threshold for GAPDH in the same reference sample. In each group, there were $n = 3$ samples.

Adenovirus vectors (Ax). STAT3 has a phosphorylation site at tyrosine705. In the dominant negative mutants of STAT3 (STAT3F), the phosphorylatable tyrosine residue is substituted with phenylalanine. Axs encoding STAT3F (AxCA STAT3F), SOCS1/JAB (AxCAJAB), and SOCS3/CIS3 (AxCACIS3) were generated as previously described [29] using the COS–TPC method [30]. Ax encoding lacZ (Ax LacZ) was a gift from Dr. Izumi Saito (University of Tokyo). Virus stocks were prepared using a standard procedure [30]. Concentrated, purified virus stocks were prepared using a CsCl gradient, and the virus titer was checked using a plaque formation assay. We infected normal human keratinocytes with Ax at a multiplicity of infection (MOI) of five.

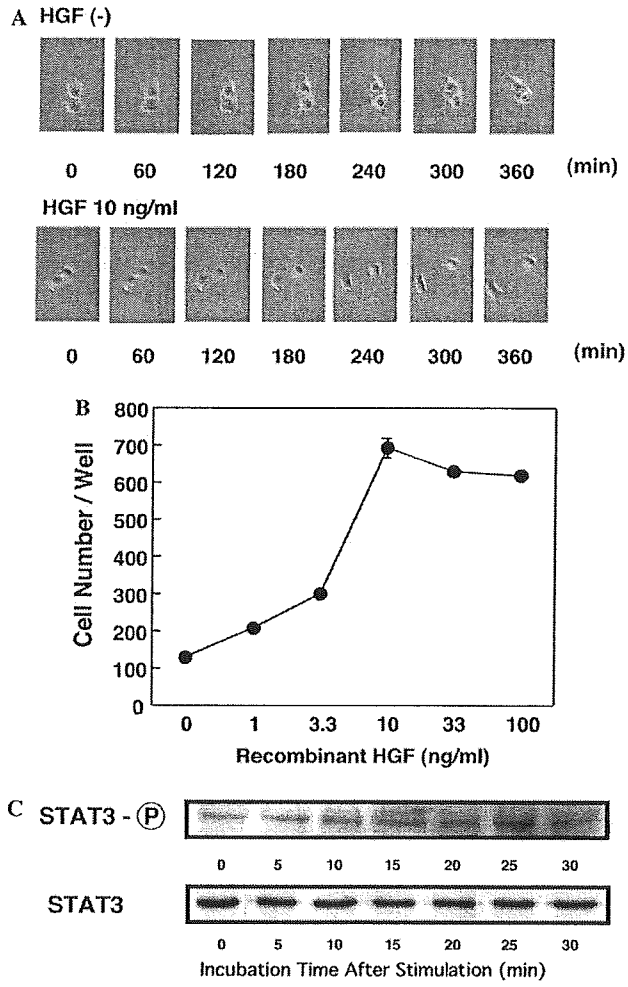

Fig. 1. Keratinocyte migration and phosphorylation of STAT3 by HGF. (A) HGF-induced keratinocyte migration. After adding 10 ng/ml HGF, keratinocyte migration was observed under time-lapse video microscopy every 60 min. (B) Quantification of keratinocyte migration induced by HGF. The indicated amount of HGF was added to the bottom wells of a 48-well Boyden chamber, and then an 8-μm pore-size polyvinylpyrrolidone-free polycarbonate membrane was placed on the wells. Keratinocytes were added to the upper wells at 5000 cells/well. After overnight incubation, the membrane was stained with Gill's hematoxylin. The number of cells that had migrated through the filter was determined by counting under a microscope. Each point shows means ± SD of quadruplicate measurements. (C) Phosphorylation of STAT3 by HGF. Subconfluent keratinocytes were starved for 2 h in BHE-free medium and stimulated with 10 ng/ml HGF. Cells were harvested and the phosphorylation of STAT3 was analyzed by Western blotting.

Results

HGF induces keratinocyte migration and phosphorylates STAT3

We first observed whether HGF induces the migration of normal human keratinocytes by using time-lapse video microscopy (Fig. 1A). Keratinocytes started to migrate within 180 min after HGF stimulation. Without HGF, no migration occurred. Then, the migration was analyzed quantitatively using the Boyden chamber assay (Fig. 1B). HGF induced keratinocyte migration sixfold that of control. The optimum concentration of HGF was 10 ng/ml. The phosphorylation of STAT3 was analyzed by Western blotting (Fig. 1C). HGF phosphorylated STAT3 at 25 min.

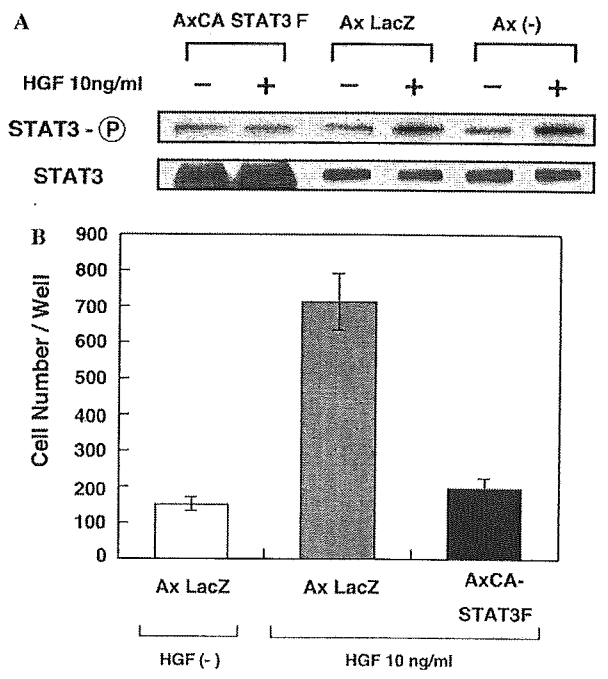

Fig. 2. Inhibition of HGF-induced phosphorylation of STAT3 and keratinocyte migration by STAT3F. (A) Inhibition of STAT3 phosphorylation. Ax LacZ and AxCA STAT3F were transfected into normal human keratinocytes at an MOI of 5. After 24 h, the keratinocytes were stimulated with 10 ng/ml HGF or vehicle alone for 25 min. Then the cells were harvested and analyzed by Western blotting. (B) Inhibition of keratinocyte migration. Ax LacZ and AxCA STAT3F were transfected into normal human keratinocytes at an MOI of five. After 24 h, the keratinocytes were harvested and transferred to a Boyden chamber and HGF (10 ng/ml) was added to the lower chamber. The migration was analyzed as in Fig. 1B. Each point shows the mean ± SD of quadruplicate measurements.

Phosphorylation of STAT3 is essential for HGF-induced keratinocyte migration

We next constructed dominant negative mutants of STAT3 (STAT3F) to study the role of STAT3 in HGF-induced keratinocyte migration. The expression of STAT3F using Ax (AxCA STAT3F) almost completely blocked HGF-induced STAT3 phosphorylation, while the transfection of LacZ had no effect on the STAT3 phosphorylation (Fig. 2A).

Using AxCA STAT3F, we analyzed the functions of STAT3 in HGF-induced keratinocyte migration. After the transfection of keratinocytes with AxCA STAT3F, the HGF-induced migration of the keratinocytes was quantitatively analyzed with the Boyden chamber assay (Fig. 2B). The expression of STAT3F almost completely blocked HGF-induced keratinocyte migration, while the expression of LacZ had no effect on migration. Because STAT3 was phosphorylated by HGF, and because HGF-induced migration was blocked by STAT3F, we concluded that the phosphorylation of STAT3 is essential for HGF-induced keratinocyte migration.

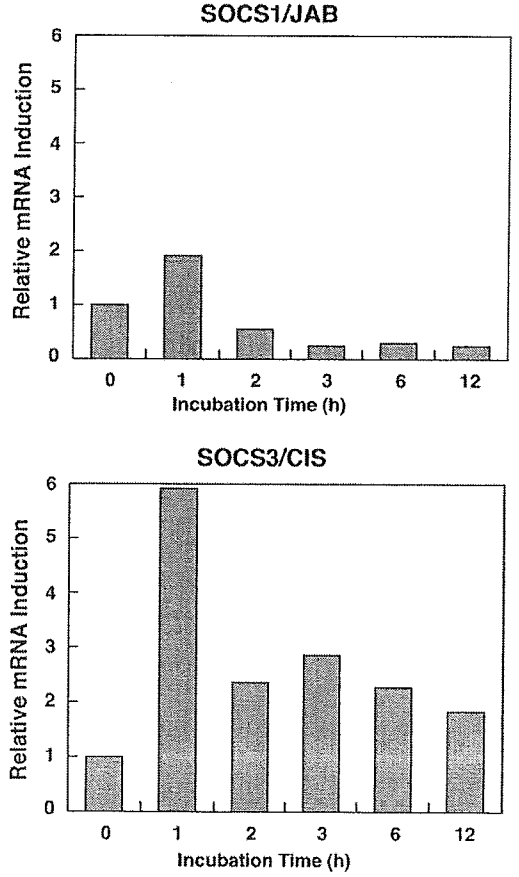

Fig. 3. Induction of SOCS3/CIS by HGF. Subconfluent keratinocytes were stimulated with 10 ng/ml HGF. Cells were harvested at the indicated time. The mRNA expression of SOCS1/JAB and SOCS3/CIS was analyzed using real-time PCR. The results were adjusted to relative values using GAPDH as an internal reference.

HGF induces SOCS3/CIS3

The SOCS/CIS family is inducible de novo by stimulation and negatively regulates the STAT family. Therefore, it is possible that the SOCS/CIS family regulates HGF-induced keratinocyte migration. To prove this, we first determined whether HGF induces the SOCS/CIS family in keratinocytes. As shown in Fig. 3, HGF enhanced the SOCS3/CIS3 mRNA expression sixfold at 1 h after stimulation, while the induction of SOCS1/JAB by HGF was not as significant as that of SOCS3/CIS3.

SOCS1/JAB and SOCS3/CIS3 inhibit HGF-induced STAT3 phosphorylation and keratinocyte migration

First, we determined the effects of SOCS1/JAB and SOCS3/CIS3 on HGF-induced STAT3 phosphorylation. AxCAJAB and AxCACIS3 were transfected into keratinocytes; the expression of either SOCS1/JAB or SOCS3 / CIS3 almost completely blocked HGF-induced STAT3 phosphorylation (Fig. 4A).

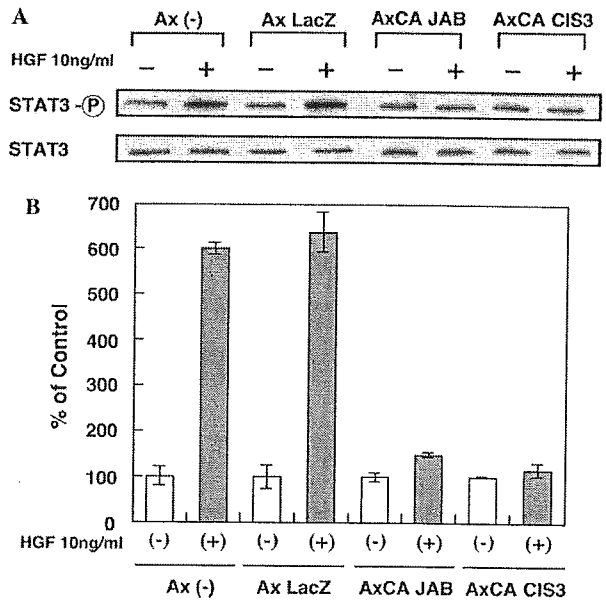

Fig. 4. Inhibition of HGF-induced STAT3 phosphorylation and keratinocyte migration by SOCS1/JAB and SOCS3/CIS3. (A) Inhibition of STAT3 phosphorylation. Ax LacZ, AxCAJAB, and AxCACIS3 were transfected into normal human keratinocytes at an MOI of 5. After 24 h, the keratinocytes were stimulated with 10 ng/ml HGF or vehicle alone for 25 min. Then, the cells were harvested and analyzed by Western blotting. (B) Inhibition of keratinocyte migration. Ax LacZ, AxCAJAB, and AxCACIS3 were transfected into normal human keratinocytes at an MOI of 5. After 24 h, the keratinocytes were harvested and transferred to a Boyden chamber for the analysis of migration, as described in Fig. 1B. HGF (10 ng/ml) was added to the lower chamber, and the set-up was incubated overnight. Each point shows the mean ± SD of quadruplicate measurements.

Using AxCAJAB and AxCACIS3, we analyzed the regulatory mechanism of STAT3 in HGF-induced keratinocyte migration. After the transfection of keratinocytes with AxCAJAB or AxCACIS3, the HGF-induced migration of the keratinocytes was analyzed quantitatively with the Boyden chamber assay (Fig. 4B). The expression of either SOCS1/JAB or SOCS3/CIS3 almost completely blocked HGF-induced keratinocyte migration. Because SOCS3/CIS3 was induced by HGF and SOCS3/CIS3 blocked HGF-induced phosphorylation of STAT3 and migration, we concluded that SOCS3/CIS3 regulates HGF-induced keratinocyte migration.

Discussion

The intracellular signaling mechanisms involving c-Met have been studied in hepatocytes primarily. Although it was demonstrated that HGF induces keratinocyte migration [8], the intracellular signaling mechanisms remained unclear. It was suggested that the major signaling pathway downstream from HGF/c-Met is the MAPK cascade [31]. However, the involvement of STAT signaling cascades in HGF-induced signal transduction was also reported [19]. Because EGF-induced keratinocyte migration was abolished in STAT3-disrupted keratinocytes [32], STAT pathways were thought to be involved in HGF-induced keratinocyte migration. Therefore, we studied whether SOCS/CIS regulates HGF-induced keratinocyte migration.

The SOCS/CIS family negatively regulates STAT pathways. However, the inhibitory functions of the SOCS/CIS family differ among cell types and cell conditions. In this study, we showed that SOCS3/CIS3 was induced and inhibited STAT3 phosphorylation and migration, indicating that SOCS3/CIS3 acts as a self-limiting factor to avoid overstimulation. Although HGF induces SOCS3/CIS3, EGF, a growth factor that strongly induces keratinocyte migration [33], does not induce SOCS1/JAB or SOCS3/CIS3 [29]. Therefore, EGF-induced keratinocyte migration does not involve the SOCS1/JAB- or SOCS3/CIS3-mediated self-regulatory mechanism of STAT3 activation in keratinocytes. This indicates that the intracellular regulatory mechanism of keratinocyte migration differs among growth factors.

In this study, we showed that SOCS1/JAB inhibited HGF-induced keratinocyte migration. However, SOCS1/JAB was not induced by HGF, suggesting that SOCS1/JAB has another role other than acting as a self-limiting factor. It is possible that cytokine-induced SOCS1/JAB or SOCS3/CIS3 affects HGF-induced keratinocyte migration. Although the inhibitory and negative regulatory mechanisms of cytokine signals in epidermal keratinocytes have not been assessed fully, cytokines such as IFN-γ, IL-4, and IL-6 are implicated in a variety of physiological and pathological conditions of the skin. IFN-γ enhances SOCS1/JAB and SOCS3/CIS3 expression [29]. In addition, IL-4 and IL-6 enhance the expression of SOCS1/JAB and SOCS3/CIS3, respectively [29]. Therefore, cytokines in various inflammatory skin conditions might affect wound healing by regulating keratinocyte migration via the induction of SOCS1/JAB or SOCS3/CIS3.

In conclusion, the SOCS3/CIS3 negative feedback mechanism of STAT3 activation is a key pathway of HGF-induced keratinocyte migration.

Acknowledgments

We thank Teruko Tsuda and Eriko Tan for their excellent technical assistance.

References

[1] Y. Sarret, D.T. Woodley, K. Grigsby, K. Wynn, E.J. O'Keefe, Human keratinocyte locomotion: the effect of selected cytokines, J. Invest. Dermatol. 98 (1992) 12–16.
[2] T. Nakamura, K. Nawa, A. Ichihara, Partial purification and characterization of hepatocyte growth factor from serum of hepatectomized rats, Biochem. Biophys. Res. Commun. 122 (1984) 1450–1459.
[3] W.E. Russell, J.A. McGowan, N.L. Bucher, Biological properties of a hepatocyte growth factor from rat platelets, J. Cell. Physiol. 119 (1984) 193–197.
[4] K. Matsumoto, T. Nakamura, Hepatocyte growth factor (HGF) as a tissue organizer for organogenesis and regeneration, Biochem. Biophys. Res. Commun. 239 (1997) 639–644.
[5] C. Birchmeier, E. Gherardi, Developmental roles of HGF/SF and its receptor, the c-Met tyrosine kinase, Trends Cell Biol. 8 (1998) 404–410.
[6] Y.W. Zhang, G.F. Vande Woude, HGF/SF-met signaling in the control of branching morphogenesis and invasion, J. Cell. Biochem. 88 (2003) 408–417.
[7] E. Gohda, H. Kataoka, H. Tsubouchi, Y. Daikilara, I. Yamamoto, Phorbol ester-induced secretion of human hepatocyte growth factor by human skin fibroblasts and its inhibition by dexamethasone, FEBS Lett. 301 (1992) 107–110.
[8] K. Matsumoto, K. Hashimoto, K. Yoshikawa, T. Nakamura, Marked stimulation of growth and motility of human keratinocytes by hepatocyte growth factor, Exp. Cell Res. 196 (1991) 114–120.
[9] R. Tsuboi, C. Sato, C.M. Shi, H. Ogawa, Stimulation of keratinocyte migration by growth factors, J. Dermatol. 19 (1992) 652–653.
[10] S. Yoshida, K. Matsumoto, D. Tomioka, K. Bessho, S. Itami, K. Yoshikawa, T. Nakamura, Recombinant hepatocyte growth factor accelerates cutaneous wound healing in a diabetic mouse model, Growth Factors 22 (2004) 111–119.
[11] K. Nakanishi, M. Uenoyama, N. Tomita, R. Morishita, Y. Kaneda, T. Ogihara, K. Matsumoto, T. Nakamura, A. Maruta, S. Matsuyama, T. Kawai, T. Aurues, T. Hayashi, T. Ikeda, Gene transfer of human hepatocyte growth factor into rat skin wounds mediated by liposomes coated with the Sendai virus (hemagglutinating virus of Japan), Am. J. Pathol. 161 (2002) 1761–1772.

[12] D. Bevan, E. Gherardi, T.P. Fan, D. Edwards, R. Warn, Diverse and potent activities of HGF/SF in skin wound repair, J. Pathol. 203 (2004) 831–838.
[13] I. Ono, T. Yamashita, T. Hida, H.Y. Jin, Y. Ito, H. Hamada, Y. Akasaka, T. Ishii, K. Jimbow, Local administration of hepatocyte growth factor gene enhances the regeneration of dermis in acute incisional wounds, J. Surg. Res. 120 (2004) 47–55.
[14] A. Graziani, D. Gramaglia, L.C. Cantley, P.M. Comoglio, The tyrosine-phosphorylated hepatocyte growth factor/scatter factor receptor associates with phosphatidylinositol 3-kinase, J. Biol. Chem. 266 (1991) 22087–22090.
[15] C. Ponzetto, A. Bardelli, Z. Zhen, F. Maina, P. dalla Zonca, S. Giordano, A. Graziani, G. Panayotou, P.M. Comoglio, A multifunctional docking site mediates signaling and transformation by the hepatocyte growth factor/scatter factor receptor family, Cell 77 (1994) 261–271.
[16] A. Bardelli, P. Longati, D. Gramaglia, M.C. Stella, P.M. Comoglio, Gab1 coupling to the HGF/Met receptor multifunctional docking site requires binding of Grb2 and correlates with the transforming potential, Oncogene 15 (1997) 3103–3111.
[17] L. Nguyen, M. Holgado-Madruga, C. Maroun, E.D. Fixman, D. Kamikura, T. Fournier, A. Charest, M.L. Tremblay, A.J. Wong, M. Park, Association of the multisubstrate docking protein Gab1 with the hepatocyte growth factor receptor requires a functional Grb2 binding site involving tyrosine 1356, J. Biol. Chem. 272 (1997) 20811–20819.
[18] C.R. Maroun, M. Holgado-Madruga, I. Royal, M.A. Naujokas, T.M. Fournier, A.J. Wong, M. Park, The Gab1 PH domain is required for localization of Gab1 at sites of cell-cell contact and epithelial morphogenesis downstream from the met receptor tyrosine kinase, Mol. Cell. Biol. 19 (1999) 1784–1799.
[19] C. Boccaccio, M. Ando, L. Tamagnone, A. Bardelli, P. Michieli, C. Battistini, P.M. Comoglio, Induction of epithelial tubules by growth factor HGF depends on the STAT pathway, Nature 391 (1998) 285–288.
[20] R.J. Duhe, L.H. Wang, W.L. Farrar, Negative regulation of Janus kinases, Cell Biochem. Biophys. 34 (2001) 17–59.
[21] A. Yoshimura, T. Ohkubo, T. Kiguchi, N.A. Jenkins, D.J. Gilbert, N.G. Copeland, T. Hara, A. Miyajima, A novel cytokine-inducible gene CIS encodes an SH2-containing protein that binds to tyrosine-phosphorylated interleukin 3 and erythropoietin receptors, EMBO J. 14 (1995) 2816–2826.
[22] T.A. Endo, M. Masuhara, M. Yokouchi, R. Suzuki, H. Sakamoto, K. Mitsui, A. Matsumoto, S. Tanimura, M. Ohtsubo, H. Misawa, T. Miyazaki, N. Leonor, T. Taniguchi, T. Fujita, Y. Kanakura, S. Komiya, A. Yoshimura, A new protein containing an SH2 domain that inhibits JAK kinases, Nature 387 (1997) 921–924.
[23] T. Naka, M. Narazaki, M. Hirata, T. Matsumoto, S. Minamoto, A. Aono, N. Nishimoto, T. Kajita, T. Taga, K. Yoshizaki, S. Akira, T. Kishimoto, Structure and function of a new STAT-induced STAT inhibitor, Nature 387 (1997) 924–929.
[24] H. Yasukawa, H. Misawa, H. Sakamoto, M. Masuhara, A. Sasaki, T. Wakioka, S. Ohtsuka, T. Imaizumi, T. Matsuda, J.N. Ihle, A. Yoshimura, The JAK-binding protein JAB inhibits Janus tyrosine kinase activity through binding in the activation loop, EMBO J. 18 (1999) 1309–1320.
[25] W.S. Alexander, R. Starr, J.E. Fenner, C.L. Scott, E. Handman, N.S. Sprigg, J.E. Corbin, A.L. Cornish, R. Darwiche, C.M. Owczarek, T.W. Kay, N.A. Nicola, P.J. Hertzog, D. Metcalf, D.J. Hilton, SOCS1 is a critical inhibitor of interferon gamma signaling and prevents the potentially fatal neonatal actions of this cytokine, Cell 98 (1999) 597–608.
[26] D. Metcalf, C.J. Greenhalgh, E. Viney, T.A. Willson, R. Starr, N.A. Nicola, D.J. Hilton, W.S. Alexander, Gigantism in mice lacking suppressor of cytokine signalling-2, Nature 405 (2000) 1069–1073.
[27] K. Midorikawa, K. Sayama, Y. Shirakata, Y. Hanakawa, L. Sun, K. Hashimoto, Expression of vitamin D receptor in cultured human keratinocytes and fibroblasts is not altered by corticosteroids, J. Dermatol. Sci. 21 (1999) 8–12.
[28] S. Boyden, The chemotactic effect of mixtures of antibody and antigen on polymorphonuclear leucocytes, J. Exp. Med. 115 (1962) 453–466.
[29] K. Yamasaki, Y. Hanakawa, S. Tokumaru, Y. Shirakata, K. Sayama, T. Hanada, A. Yoshimura, K. Hashimoto, Suppressor of cytokine signaling 1/JAB and suppressor of cytokine signaling 3/cytokine-inducible SH2 containing protein 3 negatively regulate the signal transducers and activators of transcription signaling pathway in normal human epidermal keratinocytes, J. Invest. Dermatol. 120 (2003) 571–580.
[30] S. Miyake, M. Makimura, Y. Kanegae, S. Harada, Y. Sato, K. Takamori, C. Tokuda, I. Saito, Efficient generation of recombinant adenoviruses using adenovirus DNA-terminal protein complex and a cosmid bearing the full-length virus genome, Proc. Natl. Acad. Sci. USA 93 (1996) 1320–1324.
[31] D. Tulasne, R. Paumelle, K.M. Weidner, B. Vandenbunder, V. Fafeur, The multisubstrate docking site of the MET receptor is dispensable for MET-mediated RAS signaling and cell scattering, Mol. Biol. Cell 10 (1999) 551–565.
[32] S. Sano, S. Itami, K. Takeda, M. Tarutani, Y. Yamaguchi, H. Miura, K. Yoshikawa, S. Akira, J. Takeda, Keratinocyte-specific ablation of Stat3 exhibits impaired skin remodeling, but does not affect skin morphogenesis, EMBO J. 18 (1999) 4657–4668.
[33] Y. Ando, P.J. Jensen, Epidermal growth factor and insulin-like growth factor I enhance keratinocyte migration, J. Invest. Dermatol. 100 (1993) 633–639.

Heparin-binding EGF-like growth factor accelerates keratinocyte migration and skin wound healing

Yuji Shirakata[1,*,‡], Rina Kimura[2,*], Daisuke Nanba[3], Ryo Iwamoto[2], Sho Tokumaru[1], Chie Morimoto[3], Koichi Yokota[4], Masanori Nakamura[4], Koji Sayama[1], Eisuke Mekada[2], Shigeki Higashiyama[3] and Koji Hashimoto[1]

[1]Department of Dermatology, Ehime University School of Medicine, Ehime 791-0295, Japan
[2]Research Institute for Microbial Diseases, Osaka University, Osaka 565-0871, Japan
[3]Biochemistry and Molecular Genetics, Ehime University School of Medicine, Ehime 791-0295, Japan
[4]Carna Biosciences Incorporated, Kobe, Hyogo 650-0047, Japan
*These authors contributed equally to this work
‡Author for correspondence (e-mail: shirakat@m.ehime-u.ac.jp)

Accepted 14 February 2005
Journal of Cell Science 118, 2363-2370 Published by The Company of Biologists 2005
doi:10.1242/jcs.02346

Summary

Members of the epidermal growth factor (EGF) family are the most important growth factors involved in epithelialization during cutaneous wound healing. Heparin-binding EGF-like growth factor (HB-EGF), a member of the EGF family, is thought to play an important role in skin wound healing. To investigate the in vivo function of HB-EGF in skin wound healing, we generated keratinocyte-specific HB-EGF-deficient mice using Cre/loxP technology in combination with the keratin 5 promoter. Studies of wound healing revealed that wound closure was markedly impaired in keratinocyte-specific HB-EGF-deficient mice. HB-EGF mRNA was upregulated at the migrating epidermal edge, although cell growth was not altered. Of the members of the EGF family, HB-EGF mRNA expression was induced the most rapidly and dramatically as a result of scraping in vitro. Combined, these findings clearly demonstrate, for the first time, that HB-EGF is the predominant growth factor involved in epithelialization in skin wound healing in vivo and that it functions by accelerating keratinocyte migration, rather than proliferation.

Key words: Conditional knockout, HB-EGF, Keratinocytes, Migration, Wound healing

Introduction

Cutaneous wound healing requires precise coordination of epithelialization, dermal repair and angiogenesis (Singer and Clark, 1999). Epithelialization is ultimately dependent on the migratory, proliferative and differentiation abilities of keratinocytes. The growth and differentiation of keratinocytes are regulated mainly by a variety of growth factors (Hashimoto, 2000), of which the members of the epidermal growth factor (EGF) family are the most important for skin wound healing.

The EGF family consists of EGF, transforming growth factor (TGF)-α, heparin binding EGF-like growth factor (HB-EGF), amphiregulin (AR), epiregulin (EPR), betacellulin (BTC), epigen and neuregulin (NRG)-1, NRG-2, NRG-3 and NRG-4 (Falls, 2003; Harari et al., 1999). The EGF receptor (EGFR) family consists of EGFR (also called ErbB1), ErbB2, ErbB3 and ErbB4 (Jorissen et al., 2003). The mammalian ligands that bind EGFR include EGF, HB-EGF, TGF-α, AR, BTC, EPR and epigen. Recent studies using gene targeting or transgenic models have revealed that EGFR is essential for epithelial development in the skin, lung and gastrointestinal tract, whereas ErbB2, ErbB3, ErbB4 and neuregulins are essential for the development of cardiac muscle and the central nervous system (Erickson et al., 1997; Gassmann et al., 1995; Lee et al., 1995; Meyer and Birchmeier, 1995; Miettinen et al., 1995; Murillas et al., 1995; Riethmacher et al., 1997; Sibilia and Wagner, 1995).

Previous reports have shown that TGF-α, AR, HB-EGF and EPR are autocrine growth factors in normal human epidermal keratinocytes (NHEK) (Coffey et al., 1987; Cook et al., 1991; Hashimoto et al., 1994; Shirakata et al., 2000). It has been reported that keratinocyte migration and proliferation are predominantly mediated by autocrine EGFR activation (Stoll et al., 1997). However, the importance of the role that the EGF family plays in skin wound healing has not been confirmed in vivo using knockout mice. Previously, Marikovsky et al. (Marikovsky et al., 1993) reported that HB-EGF is a major component of the mix of growth factors found in wound fluid. Therefore, we speculated that HB-EGF was an important member of the EGF family in cutaneous wound healing. To test this hypothesis, we generated keratinocyte-specific HB-EGF knockout mice, and clearly demonstrated that HB-EGF is an important growth factor for epithelialization in skin wound healing in vivo.

Materials and Methods

Cell culture

Normal human epidermal keratinocytes (NHEK) were prepared and cultured under serum-free conditions, as previously described (Shirakata et al., 2000; Shirakata et al., 2003). Third- or fourth-passage cells were used in this study.

Table 1. Primer sequences for PCR

Wild-type HB-EGF – upper	5′-CATGATGCTCCAGTGAGTAGGCTCTGATTAC
Wild-type HB-EGF – lower	5′-AGGGCAAGATCATGTGTCCTGCCTCAAGCC
lox HB-EGF – upper	5′-ATGGGATCGGCCATTGAACA
lox HB-EGF – lower	5′-GAAGAACTCGTCAAGAAGGC
cre-recombinase – upper	5′-TTACCGGTCGATGCAACGAGTGATG
cre-recombinase – lower	5′-TTCCATGAGTGAACGAACCTGGTCG
lox-out HB-EGF – upper	5′-CGGACAGTGCCTTAGTGGAACCTC
lox-out HB-EGF – lower	5′-GCTTCTTCTTAGGAGGGATCTTGGC

Table 2. Primer sequences for RT-PCR

hHB-EGF – upper	5′-CCACACCAAACAAGGAGGAG
hHB-EGF – lower	5′-ATGAGAAGCCCCACGATGAC
hEPR – upper	5′-TCGCCCGCTCCCATCGCCG
hEPR – lower	5′-GGTTCCACATATTATTTCTG
hTGF-α – upper	5′-GAGTGCAGACCCGCCCGTGGC
hTGF-α – lower	5′-CCAGGAGGTCCGCATGCTCAC
hAR – upper	5′-CCAAAACAAGACGGAAAGTGA
hAR – lower	5′-AGGATCACAGCAGACATAAAG
hGAPDH – upper	5′-ACCACAGTCCATGCCATCAC
hGAPDH – lower	5′-TCCACCACCCTGTTGCTGTA
mHB-EGF – upper	5′-GGAATTCTGGAGCGGCTTCGGAGAG
mHB-EGF – lower	5′-CAAGCTTTGCAAGAGGGAGTACGGAACT
mEPR – upper	5′-GGAATTCTGACGCTGCTTTGTCTAGGTT
mEPR – lower	5′-CAAGCTTTATGCATCCAGCGGTTATGAT
mTGF-α – upper	5′-GGAATTCCTAGCGCTGGGTATCCTGTTA
mTGF-α – lower	5′-CAAGCTTACCACCACCAGGGCAGTGATG
mAR – upper	5′-CAAGCTTACCACCACCAGGGCAGTGATG
mAR – lower	5′-CAAGCTTACCACCACCAGGGCAGTGATG

h, human; m, mouse; EPR, epiregulin; AR, amphiregulin.

Generation of HB-EGF knockout mice using a gene targeting Cre-loxP strategy and PCR

The targeting construct has been described previously (Iwamoto et al., 2003). Homozygous $HB^{lox/lox}$ mice were bred with K5 promoter-driven Cre-recombinase transgenic mice to generate K5-Cre-$HB^{lox/+}$ mice (Takeda et al., 2000). Subsequently, K5-Cre-$HB^{lox/+}$ mice were bred with $HB^{lox/lox}$ mice to generate $HB^{lox/lox}$: K5-Cre ($HB^{-/-}$) mice. The genotype of each mouse was confirmed by PCR. Primers are shown in Table 1.

RT-PCR analysis

Keratinocytes were cultured in MCDB153 complete medium on type I collagen-coated dishes until they reached confluency. Keratinocytes were treated by tip scraping and total RNA was harvested at several time points. mRNA expression of HB-EGF, TGF-α, AR, EPR and GAPDH was analyzed by RT-PCR. The absence of HB-EGF mRNA in keratinocytes from $HB^{-/-}$ mice was confirmed by RT-PCR. Primers are shown in Table 2. The RT-PCR was performed using RT-PCR High Plus (Toyobo Co. Ltd, Osaka, Japan) according to the manufacturer's instructions. cDNA was reverse-transcribed from total RNA for 30 minutes at 60°C and heated to 94°C for 2 minutes. Amplification was performed using a DNA thermal cycler (Astec, Fukuoka, Japan) for 25 cycles. A cycle profile consisted of 1 minute at 94°C for denaturation, 1.5 minutes at 60°C for annealing and primer extension.

Wound healing studies

Wound healing experiments were performed in $HB^{-/-}$ and $HB^{lox/lox}$ mice. Under sodium pentobarbital anesthesia, two full-thickness wounds were created on the skin of the backs of each of nine 9- to 10-week-old female mice using 6-mm skin biopsy punches. Each wound diameter was determined as the average of longitudinal and lateral diameter. Wound closure was monitored, and skin sections were harvested at 3, 5, 7, 9 and 11 days after wounding. For BrdU labeling, mice received intraperitoneal injections of BrdU (250 μg/g; Sigma, Tokyo, Japan) 2 hours prior to sacrifice.

Histological analysis

Mouse tissues were fixed in 4% paraformaldehyde or formaldehyde, dehydrated and embedded in paraffin. Four-μm sections were stained with Hematoxylin and Eosin. For β-gal staining, after fixation with 0.2% glutaraldehyde and 1% formalin, the tissues were stained with 5-bromo-4-chloro-3-indol β-D-galactoside (X-gal). Skin sections were stained with rabbit anti-keratin IgG or anti-BrdU IgG, and immunopositive reactions were visualized using a streptavidin-biotin-peroxidase staining kit (Nichirei Co. Inc., Tokyo, Japan) according to the manufacturer's instructions. Morphometric analysis was performed using MacSCOPE Ver2.61 software. Statistical analysis was performed using Student's *t*-test.

Results

HB-EGF mRNA induction after in vitro scrape wound

To investigate the distinct role of HB-EGF in skin wound healing of the growth factors produced by NHEK, we first examined the induction of EGFR-ligand mRNA in NHEK in an in vitro wound-healing model. Confluent cultures of NHEK were scraped with a yellow pipette tip; total RNA was harvested at several time points, and the expression of growth-factor mRNAs was analyzed by RT-PCR. HB-EGF mRNA was rapidly induced after scraping, reaching a peak of 2.6-fold induction at 1 hour, whereas AR, TGF-α and EPR mRNAs were only slightly induced, with a maximum 1.5-fold increase (Fig. 1A). This indicates that HB-EGF is the most inducible gene of the EGFR ligands in NHEK. In normal mouse keratinocytes, HB-EGF was again the EGF family member that was induced predominantly after scraping, with a maximum 4.0-fold increase at 2 hours (Fig. 1B). EPR was also induced to a lesser degree, with a maximum 2.5-fold induction. TGF-α and AR were not induced after scraping. These results indicated that HB-EGF may play an important role in skin wound healing, and led us to investigate the in vivo function of HB-EGF.

Generation of keratinocyte-specific HB-EGF-deficient mice

Since germline targeting of the HB-EGF gene resulted in severe lethality (Iwamoto et al., 2003), we generated keratinocyte-specific HB-EGF-deficient mice ($HB^{lox/lox}$: K5-Cre, which we refer to as $HB^{-/-}$) using Cre/loxP technology in combination with the keratin 5 promoter (Takeda et al., 2000). $HB^{-/-}$ mice were identified by PCR analysis (Fig. 2A-C). The keratinocyte-specific absence of HB-EGF mRNA in $HB^{-/-}$

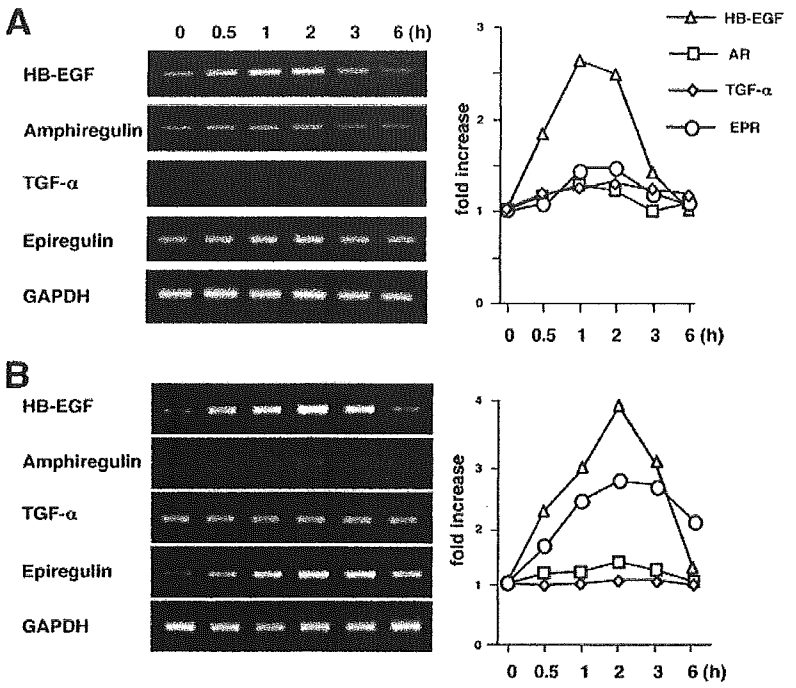

Fig. 1. Induction of expression of EGFR ligand mRNA, by scraping, in human and mouse keratinocytes. Confluent NHEK (A) and normal mouse epidermal keratinocytes (B) were scraped with a pipette tip; total RNA was harvested at several time points and mRNA expression was analyzed by RT-PCR. Right panels show densitometric analysis. In both cell types HB-EGF mRNA was rapidly and dramatically induced after scraping, whereas TGF-α, AR, and EPR mRNA were slightly induced in NHEK and the normal keratinocytes, although in the latter cells EPR was also increased.

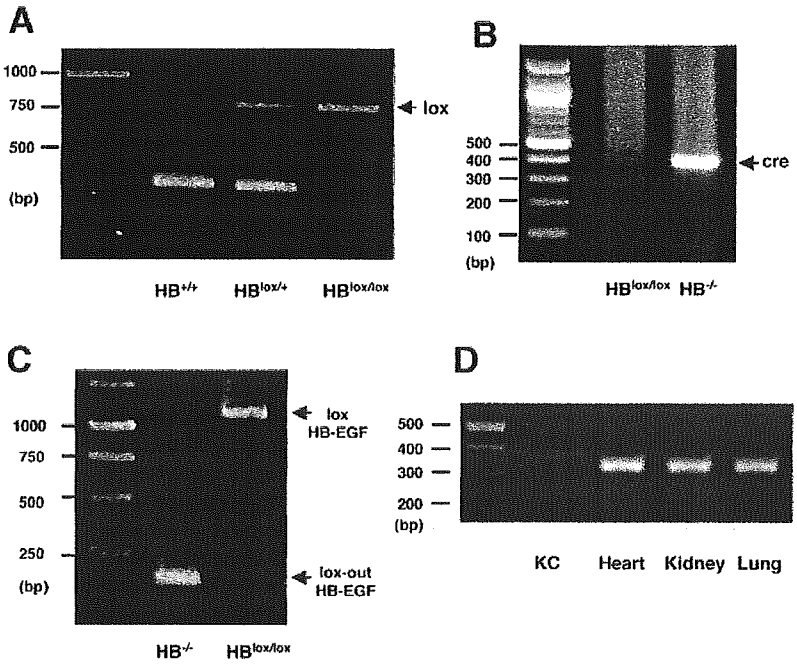

Fig. 2. Genotype of the keratinocyte-specific HB-EGF-deficient mice. (A-C) Keratinocyte-specific HB-EGF-deficient mice were confirmed by PCR as lox homozygous (A), Cre-recombinase positive (B) and lox-out (C). (D) Keratinocyte-specific disruption of HB-EGF mRNA in $HB^{-/-}$ mice was confirmed by RT-PCR. KC, keratinocytes.

mice was confirmed by RT-PCR (Fig. 2D). No apparent abnormalities were observed in the $HB^{-/-}$ mice.

Impaired wound healing in keratinocyte-specific HB-EGF-deficient mice

To examine the role of HB-EGF in skin wound healing in vivo, we performed a wound-healing assay using $HB^{lox/lox}$ and $HB^{-/-}$ mice. Two 6-mm punch skin biopsies were made in the back of each mouse and the wound diameter was measured at various times after wounding as a measure of healing. There was no difference in wound diameter up to day 3 post-wounding; however, wound healing was noticeably retarded from day 5 to 11 in the $HB^{-/-}$ mice. Wound closure was delayed significantly in $HB^{-/-}$ mice compared with $HB^{lox/lox}$ mice on day 8 (Fig. 3A). The wound diameter was reduced to 34% in $HB^{lox/lox}$ mice on day 8, whereas it was still 58% in the $HB^{-/-}$ mice (Fig. 3B). These results indicate that HB-EGF expression by keratinocytes is important for skin wound healing in vivo.

Cell proliferation was not impaired at the wound site in HB-/- mice

Since EGFR ligands promote NHEK proliferation and migration (Hashimoto, 2000), we investigated whether proliferation or migration was predominantly impaired in $HB^{-/-}$ mice. We measured the cell numbers in the leading edge of the biopsy wound and in the peripheral skin (1.2 mm from the wound margin) in $HB^{lox/lox}$ and $HB^{-/-}$ mice (Fig. 4A). After 48 hours, the total cells numbers were 90±13 and 65±19 in $HB^{lox/lox}$ and $HB^{-/-}$ mice, respectively, and after 72 hours 170±20 and 140±41 in $HB^{lox/lox}$ and $HB^{-/-}$, respectively (Fig. 4B). Since these small observed differences in cell numbers were not statistically significant, we investigated keratinocyte proliferation in $HB^{lox/lox}$ and $HB^{-/-}$ mice using a BrdU incorporation assay. Two hours before sacrifice, the mice received intraperitoneal injections of BrdU (250 μg/g). Skin samples were harvested, sectioned and stained with anti-BrdU antibody. Three days after wounding, there were no differences in the number or distribution of BrdU-positive cells between the $HB^{lox/lox}$ and $HB^{-/-}$ mice (Fig. 4C). These results suggest that delayed wound healing in $HB^{-/-}$ mice is not due to impaired cell proliferation in the epidermis.

Cell migration was impaired at the wound site in $HB^{-/-}$ mice

Since no impairment of proliferation was found, we next investigated whether migration was impaired in $HB^{-/-}$ mice. To quantify the migration

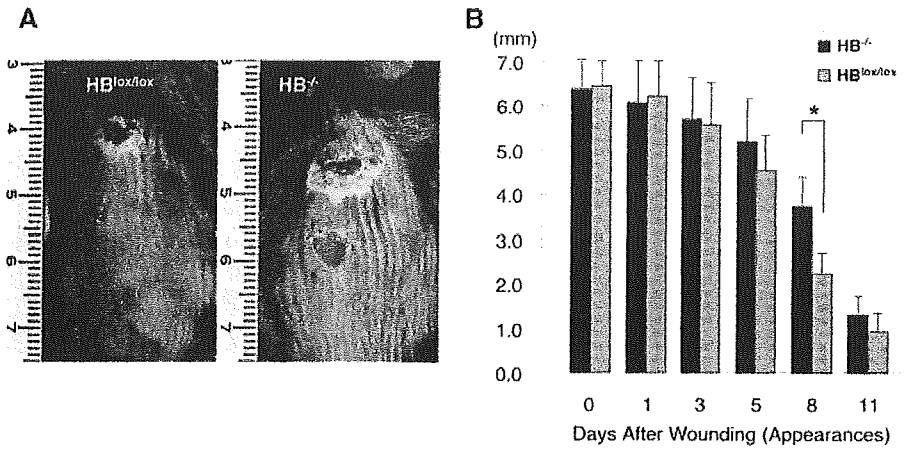

Fig. 3. Impaired wound healing in $HB^{-/-}$ mice. Two 6-mm punch biopsies were made in the skin of the backs of $HB^{lox/lox}$ and $HB^{-/-}$ mice, and wound diameter was monitored. (A) Macroscopic view of wound healing assay in $HB^{lox/lox}$ and $HB^{-/-}$ mice at day 8. (B) Measurements of wound diameter during healing. $^{*}P<0.05$.

of keratinocytes in wound healing, we measured the length of the leading edge in each wound of $HB^{lox/lox}$ and $HB^{-/-}$ mice in the wound-healing assay. Sections of skin from the wound area were stained with anti-keratin IgG (Fig. 5A). On day 7 post-wounding, the epidermis had migrated toward the center of the wound in $HB^{lox/lox}$ mice, whereas keratinocytes remained near the wound margin and the epidermis had not spread in $HB^{-/-}$ mice, suggesting that keratinocyte migration was impaired in $HB^{-/-}$ mice (Fig. 5B). We then prepared skin sections from all the samples from the wound-healing assay and calculated the ratio of leading edge to initial wound length, using computer-assisted morphometric analysis. On day 3 post-wounding, there was no difference in the leading edge ratio between $HB^{lox/lox}$ and $HB^{-/-}$ mice. However, the leading edge ratio was decreased markedly in $HB^{-/-}$ mice after day 3. The ratio was 30.7% in $HB^{-/-}$ and 44.5% in $HB^{lox/lox}$ on day 5, and 38% in $HB^{-/-}$ and 65% in $HB^{lox/lox}$ mice on day 7 (Fig. 5C). The difference on day 7 was statistically significant. These results suggest that endogenous HB-EGF is an important growth factor for the migration of epidermis in skin wound healing.

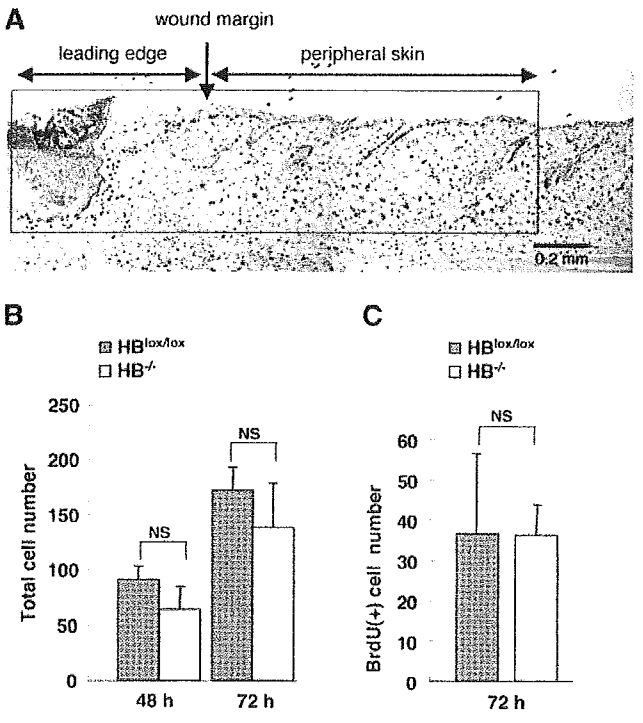

Fig. 4. BrdU-positive cell distribution at the leading edge and in the peripheral skin in $HB^{lox/lox}$ and $HB^{-/-}$ mice. (A) Skin sections were stained using anti-BrdU antibody, and cell numbers in the leading edge and in the peripheral skin were counted as indicated. (B) The total cell numbers in the peripheral skin (1.2 mm from the wound margin) and in the leading edge. (C) BrdU-positive cell number in the peripheral skin and in the leading edge. There were no differences in BrdU-positive cell numbers between $HB^{lox/lox}$ and $HB^{-/-}$ mice.

Expression of HB-EGF at wound sites

It has been reported that HB-EGF was upregulated in burn wound healing and that topical application of HB-EGF accelerated re-epithelialization of partial-thickness burns (Cribbs et al., 2002; Cribbs et al., 1998; McCarthy et al., 1996). It has been also reported that addition of HB-EGF into c-jun null keratinocyte growth medium can rescue the migration defect and induce phosphorylation of EGF receptor (Li et al., 2003). Since HB-EGF may play an important role in skin wound healing, we investigated the HB-EGF expression and keratinocyte proliferation pattern in skin wound healing using $HB^{lox/+}$:K5-Cre ($HB^{+/-}$) mice. With the targeting vector containing the *lacZ* gene as a reporter for the expression of HB-EGF, it is possible to ascertain the expression of HB-EGF by staining for β-gal in $HB^{+/-}$ mice. HB-EGF was expressed at the leading edge of the epithelium at day 2 post-wounding, and was predominantly expressed at the tip of the leading edge until day 7 (Fig. 6A). Unlike the HB-EGF expression pattern, BrdU-positive (BrdU+) cells were detected mainly within the peripheral skin on days 2 and 3. On days 5 and 7, BrdU+ cells were found toward the leading edge, although they were preferentially located near the wound margin. To quantify the distribution of HB-EGF-expressing cells and proliferating cells, we counted the β-gal-positive (β-gal+) cells and BrdU+ cells in 0.2 mm ranges in the leading edge and in the peripheral skin in $HB^{+/-}$ mice. On day 2 the peak of the β-gal+ cells was between 0 +0.2 mm into the leading edge, whereas the peak of the BrdU+ cells was –0.2 to –0.4 mm into the peripheral skin. On day 3, the peak of the β-gal+ cells was between +0.4 and +0.6 mm, whereas the peak of the BrdU+ cells was between 0

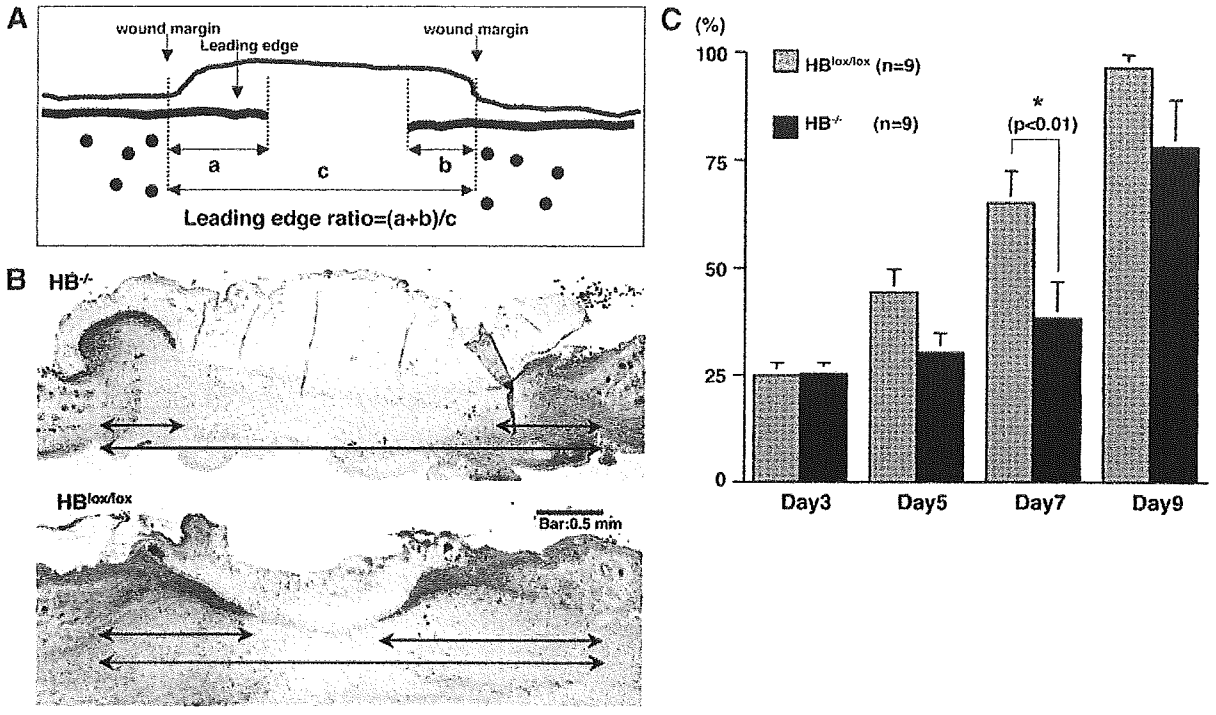

Fig. 5. Impaired keratinocyte migration in $HB^{-/-}$ mice. (A) Serial sections were prepared, and the epidermis was stained with anti-keratin antibody. Computer-assisted morphometric analysis was performed and the ratio of the leading edge to initial wound length was calculated. (B) Immunohistochemical staining of wound healing assay at day 7. Scale bar: 500 μm. (C) Measurements of leading edge ratio in $HB^{lox/lox}$ and $HB^{-/-}$ mice. The leading edge ratio was significantly decreased in $HB^{-/-}$ mice (n=9) at day 7. *P<0.01.

and +0.2 mm. From day 5 to day 7, BrdU+ cells were located at the leading edge, although they always appeared just behind the β-gal+ cells (Fig. 6B,C).

We also examined β-gal+ and BrdU+ cells in the wound-healing assay using $HB^{-/-}$ mice. As in $HB^{+/-}$ mice, in $HB^{-/-}$ mice, on day 2 post-wounding, β-gal+ cells were localized mostly 0 to +0.2 mm into the leading edge, whereas BrdU+ cells were detected mostly between –0.2 and –0.4 mm into the peripheral skin. On day 3, the peak of the β-gal+ cells were localized at 0 to +0.2 mm, whereas the peak of the BrdU+ cells were between 0 and –0.2 mm. On days 5 and 7, the peak aggregation of BrdU+ cells in $HB^{-/-}$ mice was at almost the same location as the β-gal+ cells, at the leading edge (Fig. 6D,E). The overlapping distribution patterns of BrdU+ and β-gal+ cells in these mice may be due to the impaired cell migration (Fig. 5B,C). However, the total counts of BrdU+ cells were similar in $HB^{lox/lox}$ and $HB^{-/-}$ mice (Fig. 4B,C).

Discussion

Wound healing is a complex process involving a number of coordinated events including inflammation, cell migration, cell proliferation, matrix production and angiogenesis (Singer and Clark, 1999). A complex array of cells, growth factors, cytokines and matrix components are involved in wound healing, and a number of transgenic and knockout mouse models have revealed the contribution of several molecules to wound healing (Scheid et al., 2000). Impaired wound healing was observed in mice transgenic for several molecules, such as BMP-6, follistatin, truncated FGF receptor and thorombospondin-1, as well as in mice with activin, β1 integrin, and TGF-β1 knockouts, among others (Grose and Werner, 2003; Scheid et al., 2000; Werner and Grose, 2003). EGF family members such as EGF, TGF-α, HB-EGF, amphiregulin, betacellulin, epiregulin and their receptor EGFR mainly regulate migration, proliferation and differentiation of many cell types involved in wound healing. EGFR knockout mice showed striking abnormalities, such as wavy hair and thin skin (Miettinen et al., 1995; Sibilia and Wagner, 1995). In contrast to this striking phenotype in EGFR knockout mice, EGF-disrupted mice showed no phenotypic abnormalities (Luetteke et al., 1999). No differences in wound healing were found in TGF-α knockout mice with either excisional dorsal wounding or ear-punch wounding (Luetteke et al., 1993; Mann et al., 1993). These unexpectedly minor differences in phenotypes in wound healing in EGFR-ligand knockout mice are probably due to the known functional redundancy among the EGF family members, including HB-EGF.

HB-EGF is produced and secreted by human keratinocytes and acts as an autocrine growth factor (Hashimoto et al., 1994). HB-EGF mRNA was rapidly and dramatically induced after scrape-wounding, although slight increases in TGF-α, amphiregulin and epiregulin mRNAs were observed. Furthermore, blocking HB-EGF by addition of neutralizing antibody to the medium inhibited keratinocyte migration (Tokumaru et al., 2000). In contrast, the addition of recombinant HB-EGF to the medium accelerates keratinocyte migration (Tokumaru et al., 2000). These results indicate that

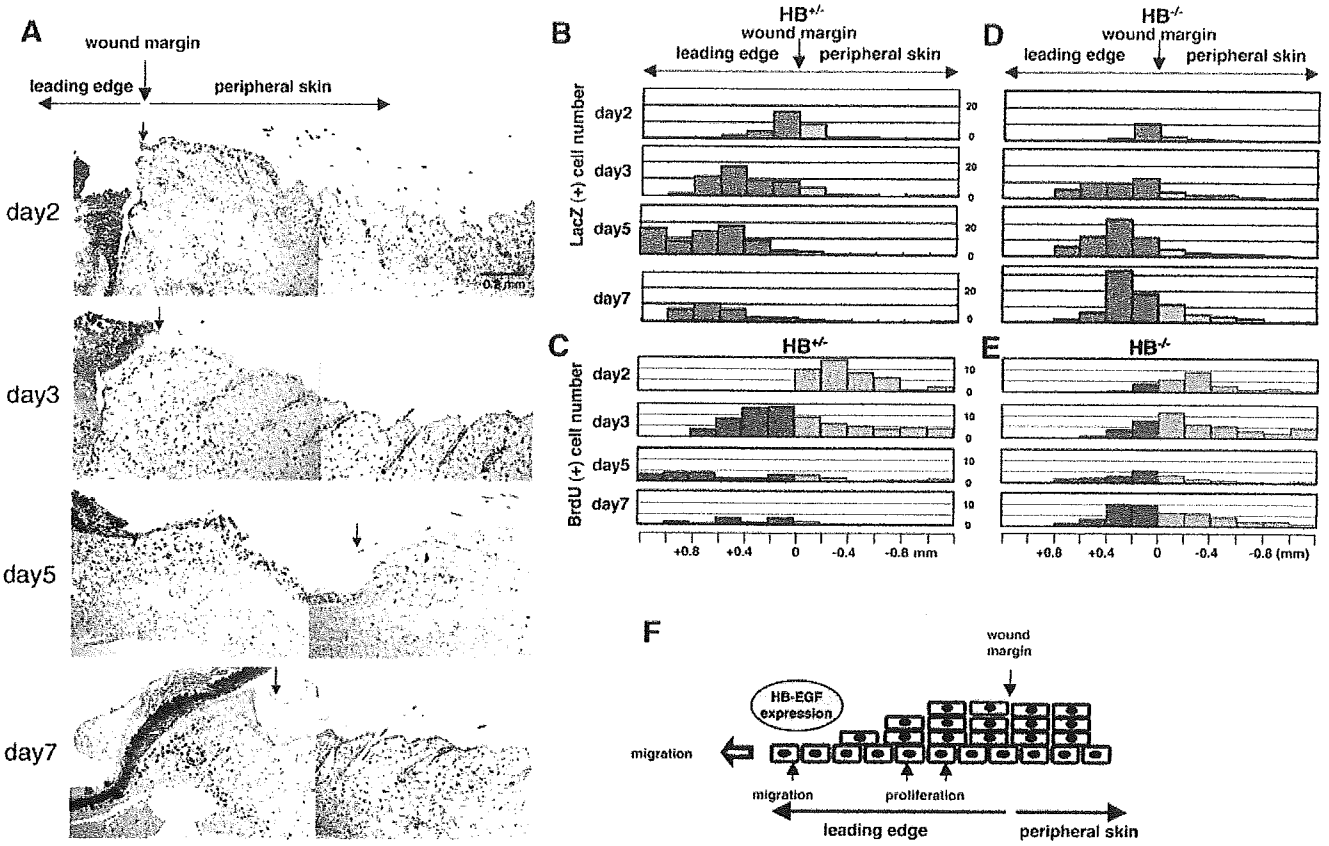

Fig. 6. HB-EGF expression in skin wound healing. The targeting vector contained the *lacZ* gene as a reporter for the expression of HB-EGF. When HB-EGF cDNA is deleted by Cre-recombinase, HB-EGF expression can be identified by X-gal staining in $HB^{+/-}$ mice. (A) Double staining for X-gal and BrdU at the wound healing stage. Scale bar: 0.2 mm. Arrow, wound margin. (B-E) Distribution of β-gal-positive [lacZ(+)] cells (B) and BrdU-positive cells (C) from day 2 to 7 in $HB^{+/-}$ mice. HB-EGF is expressed predominantly at the tip of the leading edge, whereas BrdU-positive cells were distributed mainly at wound margin. Distribution of β-gal-positive cells (D) and BrdU-positive cells (E) in $HB^{-/-}$ mice. There was no significant difference in the number of BrdU-positive cells between $HB^{+/-}$ and $HB^{-/-}$ mice at any stage of wound healing. (F) A proposed schematic illustration of skin wound healing. After injury, keratinocytes at the wound margin begin to migrate and express HB-EGF without proliferation. Next, focal release of HB-EGF may signal further migration and up-regulate HB-EGF expression in an autocrine manner. Values in B-E are number of cells per indicated area.

HB-EGF plays an important role in skin wound healing, and led us to investigate the in vivo function of HB-EGF. Since germline targeting of the HB-EGF gene resulted in embryonic lethality (Iwamoto et al., 2003), we generated keratinocyte-specific HB-EGF-deficient mice ($HB^{-/-}$) using Cre/loxP technology in combination with the keratin 5 promoter (Takeda et al., 2000). There was no difference in wound closure between $HB^{-/-}$ and $HB^{lox/lox}$ mice on day 3. However, wound closure was markedly retarded in $HB^{-/-}$ mice compared to $HB^{lox/lox}$ mice. We clearly demonstrated for the first time that endogenous HB-EGF is the most important growth factor in the epithelialization of skin wound healing in vivo, using keratinocyte-specific HB-EGF-deficient mice.

EGF family members are well known to promote keratinocyte growth in vitro (Hashimoto, 2000). It has been reported that TGF-α, amphiregulin, HB-EGF and epiregulin are autocrine growth factors in normal human keratinocytes (Coffey et al., 1987; Cook et al., 1991; Hashimoto et al., 1994; Shirakata et al., 2000). In vitro observation suggests that these EGF family members play important roles in development, epidermal morphogenesis, skin homeostasis and wound healing. In this study, we investigated HB-EGF function in cell migration and proliferation. HB-EGF stimulates keratinocyte migration in vitro and in vivo. However, there was little difference in proliferation between $HB^{lox/lox}$ and $HB^{-/-}$ mice. HB-EGF promoter activity was up-regulated at the migrating epidermal edge, whereas the distribution of proliferating cells (BrdU-positive) was not identical to that of HB-EGF mRNA-positive cells. Interestingly, the wound margin of normal epidermis expressed HB-EGF mRNA and was positive for BrdU, although HB-EGF promoter activity could not be detected in normal skin far from the wound margin. Therefore, normal skin does not require much HB-EGF, but after injury HB-EGF is induced and plays a crucial role in wound healing by up-regulating keratinocyte migration but not proliferation.

Combined, the evidence suggests that the synthesis of HB-EGF at the leading epithelial edge stimulates cells, via an autocrine loop, to migrate towards the center of the wound rather than to proliferate. Interestingly, there were few β-gal-positive cells and little HB-EGF expression in normal skin far